A Minimal Supersymmetric Model of Particle Physics and the Early Universe

W. Buchmüller [a, *], *V. Domcke* [a, †], *K. Kamada* [a, ‡] *and K. Schmitz* [b, §]

[a] Deutsches Elektronen-Synchrotron DESY, 22607 Hamburg, Germany
[b] Kavli IPMU, TODIAS, University of Tokyo, Kashiwa 277-8583, Japan

Abstract

We consider a minimal supersymmetric extension of the Standard Model, with right-handed neutrinos and local $B-L$, the difference between baryon and lepton number, a symmetry which is spontaneously broken at the scale of grand unification. To a large extent, the parameters of the model are determined by gauge and Yukawa couplings of quarks and leptons. We show that this minimal model can successfully account for the earliest phases of the cosmological evolution: Inflation is driven by the energy density of a false vacuum of unbroken $B-L$ symmetry, which ends in tachyonic preheating, i.e. the decay of the false vacuum, followed by a matter dominated phase with heavy $B-L$ Higgs bosons. Nonthermal and thermal processes produce an abundance of heavy neutrinos whose decays generate primordial entropy, baryon asymmetry via leptogenesis and dark matter consisting of gravitinos or nonthermal WIMPs. The model predicts relations between neutrino and superparticle masses and a characteristic spectrum of gravitational waves.

1 Introduction

Today we have the Standard Model of particle physics as well as the ΛCDM model of cosmology, which describe a wealth of experimental and observational data with an accuracy far beyond expectation [1]. On the other hand, despite this success, it is obvious that both standard models do not represent a final theory. The symmetry structure of the Standard Model, the smallness of neutrino masses and the discovery of a Higgs boson [2, 3] with a mass in between the vacuum stability and the triviality bound point towards grand unification as the next step beyond the Standard Model. Similarly, the parameters of the ΛCDM model, the abundance of matter and dark matter, the apparent cosmological constant and the temperature anisotropies of the cosmic microwave background ask for an explanation, which requires physics beyond the Standard Model.

Supersymmetry is an attractive framework to extrapolate the Standard Model of particle physics to the energy scale of grand unification, $\Lambda_{\rm GUT} \sim 10^{16}$GeV. It also introduces natural dark matter candidates [4–6] and scalar fields which can realize inflation, thereby providing an important link between particle physics and cosmology. Moreover, neutrino masses require right-handed neutrinos whose large Majorana masses can account for the tiny masses of the known neutrinos via the seesaw mechanism. These Majorana masses break the symmetry $B-L$, the difference between baryon and lepton number, and their decays can generate a baryon asymmetry via leptogenesis [7]. Extrapolating the feature of the Standard Model that all masses are generated by spontaneous symmetry breaking, suggests that also $B-L$ is a spontaneously broken local symmetry.

---

[*] E-mail: buchmuwi@desy.de
[†] E-mail: valerie.domcke@desy.de
[‡] E-mail: kohei.kamada@desy.de
[§] E-mail: kai.schmitz@ipmu.jp

Following these arguments we arrive at a minimal supersymmetric extension of the Standard Model, which is described by the superpotential

$$W = \sqrt{\lambda}\,\Phi\left(\frac{v_{B-L}^2}{2} - S_1 S_2\right) + \frac{1}{\sqrt{2}} h_i^n n_i^c n_i^c S_1 + h_{ij}^\nu \mathbf{5}_i^* n_j^c H_u + W_{\text{MSSM}}\,, \tag{1}$$

where S_1 and S_2 are the chiral superfields containing the Higgs field responsible for breaking $B-L$, and n_i^c denote the superfields containing the charge conjugates of the right-handed neutrinos. The symmetry-breaking sector of Eq. (1), involving the superfields S_1, S_2 and Φ, is precisely the superpotential of F-term hybrid inflation, with Φ being a singlet whose scalar component ϕ acts as the inflaton [8, 9]. v_{B-L} is the scale at which $B-L$ is broken. The $B-L$ charges are $q_S \equiv q_{S_2} = -q_{S_1} = 2$, $q_\Phi = 0$, and $q_{n_i^c} = 1$. h and λ denote coupling constants, and W_{MSSM} represents the MSSM superpotential,

$$W_{\text{MSSM}} = h_{ij}^u \mathbf{10}_i \mathbf{10}_j H_u + h_{ij}^d \mathbf{5}_i^* \mathbf{10}_j H_d\,. \tag{2}$$

For convenience, all superfields have been arranged in $SU(5)$ multiplets, $\mathbf{10} = (q, u^c, e^c)$ and $\mathbf{5}^* = (d^c, l)$, and $i, j = 1, 2, 3$ are flavour indices. We assume that the colour triplet partners of the electroweak Higgs doublets H_u and H_d have been projected out. The vacuum expection values $v_u = \langle H_u \rangle$ and $v_d = \langle H_d \rangle$ break the electroweak symmetry. In the following we will assume large $\tan\beta = v_u/v_d$, implying $v_d \ll v_u \simeq v_{\text{EW}} = \sqrt{v_u^2 + v_d^2}$. We will restrict our analysis to the case of a hierarchical heavy (s)neutrino mass spectrum, $M_1 \ll M_2, M_3$, where $M_i = h_i^n v_{B-L}$. Furthermore we assume the heavier (s)neutrino masses to be of the same order of magnitude as the common mass m_S of the particles in the symmetry-breaking sector, for definiteness we set $M_2 = M_3 = m_S$. Key parameters of the analysis are then the $B-L$ breaking scale v_{B-L}, the mass of the lightest of the heavy (s)neutrinos M_1, and the effective light neutrino mass parameter $\widetilde{m}_1$ (cf. [10]),

$$v_{B-L} \simeq \frac{v_{\text{EW}}^2}{\overline{m}_\nu}\,, \qquad M_1 \ll v_{B-L}\,, \qquad \widetilde{m}_1 \equiv \frac{(h^{\nu\dagger} h^\nu)_{11} v_{\text{EW}}^2}{M_1}\,. \tag{3}$$

Here, $\overline{m}_\nu = \sqrt{m_2 m_3} \sim 3 \times 10^{-2}\text{eV}$ is the geometric mean of the two light neutrino mass eigenvalues m_2 and m_3, and characterizes the light neutrino mass scale. In addition to the chiral superfields, the model also contains a vector supermultiplet V ensuring invariance under local $B-L$ transformations and the gravity supermultiplet consisting of the graviton G and the gravitino $\tilde{G}$.

In the following sections we shall show that this Minimal Supersymmetric Model (MSM), whose parameters are largely fixed by low energy experiments, provides a consistent description of the transition from an inflationary phase to the hot early universe. During this 'pre- and reheating' process the matter-antimatter asymmetry and the dark matter abundance are generated. Most of our discussion will be based on Refs. [10–12].

Our work is closely related to previous studies of thermal leptogenesis [13, 14] and nonthermal leptogenesis via inflaton decay [15–18], where the inflaton lifetime determines the reheating temperature. In supersymmetric models with global $B-L$ symmetry the scalar superpartner $\widetilde{N}_1$ of the lightest heavy Majorana neutrino N_1 can play the role of the inflaton in chaotic [19,20] or hybrid [21,22] inflation models. Local $B-L$ breaking in connection with hybrid, shifted hybrid and smooth hybrid inflation has been considered in Ref. [23]. One of the main motivations for nonthermal leptogenesis has been that the 'gravitino problem' for heavy unstable gravitinos [24–28] can be avoided by means of a low reheating temperature. In the following we shall assume that the gravitino is either the lightest superparticle (LSP) or very heavy, $m_{3/2} \gtrsim 10$ TeV. In the first case, gravitinos, thermally produced at a reheating temperature compatible with leptogenesis, can explain the observed dark matter abundance [29]. For very heavy gravitinos, thermal production and subsequent decay into a wino or higgsino LSP can yield nonthermal WIMP dark matter [30–32].

The MSM, defined in Eq. (1), postdicts the earliest phases of the cosmological evolution. The energy density of a false vacuum with unbroken $B-L$ symmetry drives inflation. Consistency with the measured amplitude of the temperature anisotropies of the cosmic microwave background fixes v_{B-L}, the scale of $B-L$ symmetry breaking, to be the GUT scale. Inflation ends by tachyonic preheating [33], i.e. the decay of the false vacuum, which sets the stage for a phase dominated by nonrelativistic matter in the form of heavy $B-L$ Higgs bosons. The further development is described by Boltzmann equations. Nonthermal and thermal processes produce an abundance of heavy neutrinos whose decays generate primordial entropy, baryon asymmetry via leptogenesis and gravitino dark matter from scatterings in the thermal bath. This whole pre- and reheating process is imprinted on the spectrum of primordial gravitational waves [34]. It is remarkable that the initial conditions of the radiation dominated phase are not free parameters of a cosmological model. Instead, they are determined by the parameters of a Lagrangian, which in principle can be measured by particle physics experiments and astrophysical observations. The consistency of hybrid inflation, leptogenesis and dark matter entails interesting relations between the lightest neutrino mass m_1, the gravitino mass and possibly wino or higgsino masses.

The paper is organized as follows. In Section 2 we discuss F-term hybrid inflation. Corrections from supersymmetry breaking lead to a two-field model which can account for all results deduced from the recently released Planck data. Section 3 deals with tachyonic preheating and the important topic of cosmic string formation, with emphasis on the current theoretical uncertainties. The description of the reheating process by means of Boltzmann equations and the resulting relations between neutrino masses and superparticle masses are the subject of Section 4. The predictions of the gravitational wave spectrum due to inflation, cosmic strings, pre- and reheating are reviewed in Section 5. Finally, observational prospects are addressed in Section 6.

2 Inflation

The superpotential of the MSM, cf. Eq. (1), allows for a phase of F-term hybrid inflation. For $|\phi| \gg v_{B-L}$, the $B-L$ Higgs fields are fixed at zero, $B-L$ is unbroken and the energy density of the universe is dominated by the false vacuum energy, $\rho_0 \simeq (\lambda/4)\, v_{B-L}^4 \equiv V_0$, generated by the non-vanishing vacuum expectation value (vev) of the auxiliary field F_ϕ and inducing spontaneous supersymmetry breaking. Here, we briefly review the dynamics and predictions of this inflation model, with particular focus on the status of F-term hybrid inflation in the light of the recent Planck results [35].

The scalar potential
At the high energy scales involved in inflation, supergravity corrections to the Lagrangian become important, resulting in a tree-level scalar F- and D-term potential given by

$$V_{\text{SUGRA}}^F = e^{K/M_P^2} \left[\sum_{\alpha\bar\beta} K^{\alpha\bar\beta}\, \mathcal{D}_\alpha W\, \mathcal{D}_{\bar\beta} W^* - 3\,\frac{|W|^2}{M_P^2} \right], \qquad V_{\text{SUGRA}}^D = \frac{1}{2}\, g^2 \left(\sum_\alpha q_\alpha\, K_\alpha\, z_\alpha \right)^2, \quad (4)$$

where $\mathcal{D}_\alpha W = W_\alpha + K_\alpha W / M_P^2$; the subscript α ($\bar\alpha$) denotes the derivative with respect to the (complex conjugate of the) scalar component z_α of the superfield Φ_α carrying the $U(1)$ gauge charge q_α, $K^{\alpha\bar\beta}$ is the inverse Kähler metric and $M_P = 2.4 \times 10^{18}$ GeV is the reduced Planck mass. For a canonical Kähler potential,

$$K = \sum_\alpha |z_\alpha|^2, \tag{5}$$

the D-term scalar potential reduces to the expression familiar from global supersymmetry, but an important supergravity contribution arises from the F-term potential, $V_{\text{SUGRA}}^F \supset |z_\alpha|^2 \rho_0 / M_P^2$. This yields large contributions to the masses of the scalar fields z_α of the theory. For the superpotential (1), this stabilizes the singlet sneutrinos and the MSSM scalars at a vanishing field value. The $B-L$ Higgs boson masses also obtain various supergravity contributions. However, these are suppressed by factors of

$(v_{B-L}/M_P)^2$ or $(\phi/M_P)^2$ compared to the leading order terms, which match the result found in global supersymmetry,

$$(m_{\pm}^S)^2 = \lambda(|\phi|^2 \pm \frac{1}{2}v_{B-L}^2)\,, \qquad (m_f^S)^2 = \lambda|\phi|^2\,. \tag{6}$$

The F-term supergravity contribution discussed above does not give a mass-term to the inflaton ϕ because after expanding e^{K/M_P^2} in Eq. (4), the term in question is cancelled by the corresponding term in $D_\phi W D_{\bar\phi} W^*$. The leading order supergravity contribution to the inflaton mass thus stems from the term proportional to $|\phi|^4 v_{B-L}^4/M_P^4$ in the scalar potential [36]. In addition, since supersymmetry is broken during inflation, we need to take the one-loop Coleman-Weinberg (CW) potential for the inflaton field into account, obtained by integrating out the heavy $B-L$ Higgs bosons,

$$V_{1l} = \frac{1}{64\pi^2} \mathrm{STr}\left[M^4\left(\ln\left(\frac{M^2}{Q^2}\right) - \frac{1}{2}\right)\right] \simeq \frac{\lambda^2 v_{B-L}^4}{64\pi^2}\left[\ln\left(\frac{2|\phi|^2}{v_{B-L}^2}\right) + \mathcal{O}\left(\frac{v_{B-L}^4}{4|\phi|^4}\right)\right]\,, \tag{7}$$

Here STr denotes the supertrace running over all degrees of freedom of S_1 and S_2. M is the corresponding mass matrix, cf. Eq. (6), and Q an appropriate renormalization scale, which we have set to $Q^2 = \lambda v_{B-L}^2/2$.

From the resulting scalar potential, $V = V_{\mathrm{SUGRA}}^{F+D} + V_{1l}$, we find the following picture: For $|\phi| > v_{B-L}/\sqrt{2}$, the Higgs fields $s_{1,2}$ are fixed at zero and the inflaton slowly rolls towards the origin. At $|\phi| = v_{B-L}/\sqrt{2}$, $(m_-^S)^2$ becomes negative, triggering a tachyonic instability. The Higgs fields acquire a vev and $B-L$ is broken. Both the Higgs (which, now that $B-L$ is broken, is best parametrized in unitary gauge as a radial degree of freedom dubbed σ' in Ref. [10], see also Ref. [37] for the explicit relation between σ' and the symmetry-breaking Higgs mass eigenstate in arbitrary gauge) and the inflaton field then quickly fall into their true vacuum, $|\phi| \to 0$ and $\sigma' \to \sqrt{2}\,v_{B-L}$, eliminating the vacuum energy contributions of the scalar potential and ending inflation.

Slow-roll inflation

In the slow-roll approximation, the dynamics of the homogeneous inflaton field is governed by $3H\dot\phi = -\partial V/\partial\phi^*$, where H denotes the Hubble parameter. For a scalar potential only depending on the absolute value of ϕ, cf. Eq. (7), we can rewrite this in terms of the radial and angular component of $\phi = \frac{1}{\sqrt{2}}\varphi e^{-i\theta}$,

$$3H\dot\varphi = -V'(\varphi)\,, \qquad \dot\theta = 0\,. \tag{8}$$

Turning to the quantum fluctuations of the inflaton field which are visible today in the CMB, we now evaluate the scalar potential and its derivatives at $\varphi = \varphi_*$, the value of φ at $N_* \approx 55$ e-folds before the end of inflation, when the reference scale commonly used to describe the CMB fluctuations left the horizon. With φ_f denoting the value of the inflaton at the end of inflation,[1] φ_* is given by

$$\varphi_*^2 \approx \varphi_f^2 + \frac{\lambda}{4\pi^2}M_P^2\,N_* \tag{9}$$

Of particular interest in the following will be the predictions from F-term hybrid inflation for the amplitude of the scalar fluctuations A_s, the scalar spectral index n_s and the tensor-to-scalar ratio r:

$$
\begin{aligned}
A_s &= \left.\frac{H^2}{8\pi^2\epsilon M_P^2}\right|_{\varphi_*} \approx \frac{1}{3}\left(\frac{v_{B-L}}{M_P}\right)^4 N_*\,, \\
n_s &= 1 - 6\epsilon + 2\eta|_{\varphi_*} \approx 1 - \frac{1}{N_*}\,, \\
r &= \frac{A_t}{A_s} = 16\epsilon\Big|_{\varphi_*} \approx \frac{\lambda}{2\pi^2}\frac{1}{N_*}\,,
\end{aligned}
\tag{10}
$$

---

[1] Here, φ_f is determined by either $m_-^S(\varphi_c) = 0$, cf. Eq. (6), or by the violation of the slow-roll condition, i.e. $|\eta(\varphi_\eta)| = 1$, cf. Eq. (11), whatever occurs earlier: $\varphi_f \approx \max\{v_{B-L}, \sqrt{\lambda}M_P/(\sqrt{8}\pi)\}$.
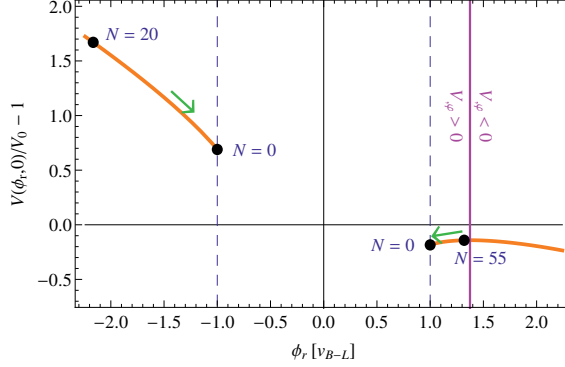
Fig. 1: Scalar potential for inflation along the real axis in the complex ϕ field space after adding a constant term W_0 to the superpotential. Slow-roll inflation is possible both for $\theta = 0$ and $\theta = \pi$. Here $\lambda = 4.5 \times 10^{-6}$, $v_{B-L} = 2.9 \times 10^{15}$ GeV and $m_{\widetilde{G}} = 47.5$ TeV.

where $A_t = 2H^2/(\pi^2 M_P^2)|_{\varphi^*}$ denotes the amplitude of the tensor fluctuations, and ϵ and η are the so-called slow-roll parameters,

$$\epsilon = \frac{M_P^2}{2}\left(\frac{V'}{V}\right)^2, \qquad \eta = M_P^2 \frac{V''}{V}. \tag{11}$$

Moreover, in Eq. (10) we have employed the the approximation[2] $\varphi_*^2 \gg \varphi_f^2$.

F-term hybrid inflation in the light of Planck
Comparing these results with the recently published Planck data [35, 38],

$$A_s = (2.18 \pm 0.05) \times 10^9, \qquad n_s = 0.963 \pm 0.0007, \qquad r < 0.26, \tag{12}$$

we find that the $B-L$ breaking scale is fixed to $v_{B-L} \approx 8 \times 10^{15}$ GeV by requiring the correct normalization of A_s, the spectral index $n_s \approx 0.98$ is rather large and the tensor-to-scalar ratio is easily below the current bound. In particular the large value for n_s has raised the question whether F-term hybrid inflation is still viable in view of the Planck results. To answer this question, we must go beyond the approximations leading to Eq. (10). First, we will drop the approximation $\varphi_*^2 \gg \varphi_f^2$, leading to corrections of the predictions listed in Eq. (10). Second, taking into account soft supersymmetry breaking, the superpotential receives a constant term $W_0 = m_{\widetilde{G}} M_P^2$ proportional to the gravitino mass [39], leading to an additional contribution to the scalar potential, studied e.g. in Refs [40, 41],

$$V_{m_{\widetilde{G}}} = -2\sqrt{\lambda}v_{B-L}^2 m_{\widetilde{G}}|\phi|\cos\theta. \tag{13}$$

This term breaks the degeneracy appearing in Eq. (7), which only depends on the absolute value $|\phi|$ of the inflaton field but not on its phase θ. As a result, the inflationary predictions found in Ref. [40] assuming $\theta = \pi$ differ from those in Ref. [41], which uses $\theta = 0$.[3] In particular, for sufficiently large $V_{m_{\widetilde{G}}}$, we find a hill-top potential for $\theta = 0$, while for $\theta = \pi$, one still finds a monotonously decreasing potential along the inflationary trajectory (along the arrows in Fig. 2), cf. Fig. 1.

Indeed, these are only two extreme cases for possible inflationary trajectories in the full two-field inflation model resulting from Eqs. (7) and (13). In the two-field model, the ending point of inflation ϕ_f becomes a 'critical line' in the complex ϕ plane, with each point on this line representing a possible

---

[2]Note that for small values of λ, the two terms in Eq. (9) can be of similar importance, leading to a slight deviation from the results listed in Eq. (10).

[3]Note that Refs. [40, 41] use a different sign convention in the superpotential, implying $\theta \to \theta + \pi$.
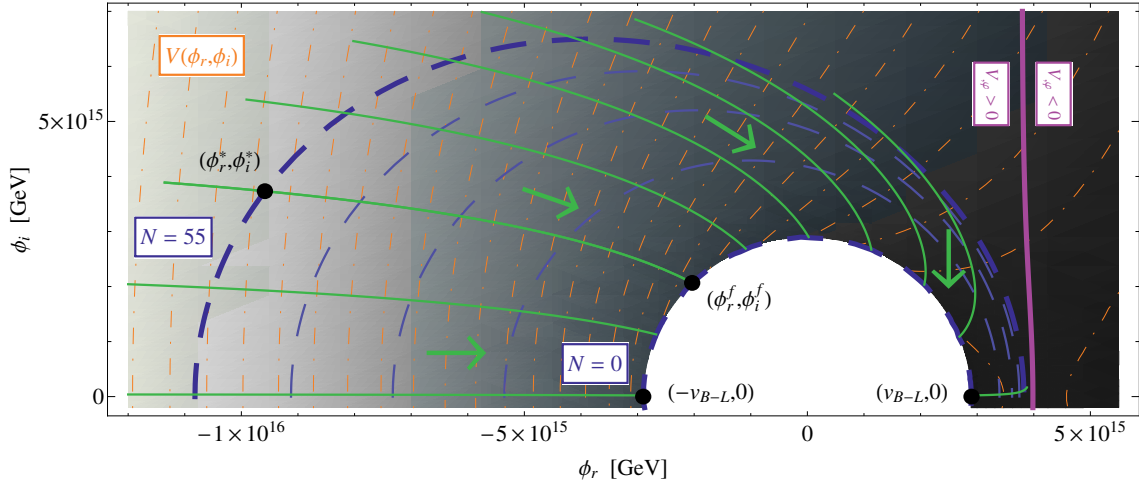
Fig. 2: Inflationary trajectories in the full two-field inflation model. Selection of possible trajectories (solid green lines) in the scalar potential $V(\phi_r, \phi_i)$ depicted by the dot-dashed orange contour lines and the shading. Lines of constant N are marked by the dashed blue contours, with the beginning and end of inflation ($N = N_*$ and $N = 0$, respectively) marked by thicker contours.

ending point for inflation. Hence as opposed to the single-field case there is an additional degree of freedom, i.e. the choice of the inflationary trajectory labeled by θ_f. This is visualized in Fig. 2 which shows a selection of possible inflationary trajectories (in green) in the scalar potential (dot-dashed orange countour lines and shading). Contour lines denoting constant numbers of e-folds N are shown as dashed blue lines, with the 'critical line', $N = 0$, and the onset of the last N_* e-folds, $N = N_{55}$ emphasized. To demonstrate the dependence of the model predictions on the choice of the trajectory, Fig. 3 shows the predictions for the amplitude A_s and the spectral index n_s as functions of the final phase θ_f for $\lambda = 4.5 \times 10^{-6}$, $v_{B-L} = 2.9 \times 10^{15}$ GeV and $m_{\widetilde{G}} = 47.5$ TeV. For this parameter example, we see that $\theta_f \simeq 16°$ reproduces the correct amplitude, cf. Eq. (12), while simultaneously yielding a value for the spectral index of $n_s = 0.965$ in very good agreement with the data.

A third possibility of manipulating Eq. (10) is by resorting to a non-minimal Kähler potential [42]. This in particular introduces a term quadratic in ϕ in the scalar potential. Tuning the expansion coefficients of such a Kähler potential, the spectral index can be tuned to lower values, achieving accordance with the Planck data even for $\theta = \pi$. However, the quadratic term then comes with a negative sign, implying, together with the positive $|\phi|^4$ term the existence of a hill-top potential and a local minimum at $|\phi| \neq 0$ where the inflaton can get trapped. Avoiding this requires some fine-tuning in the initial conditions for $|\phi|$ [40].

On top of that, there are also further constraints which must be taken into account in a realistic model. First, the superpotential Eq. (1) will lead to the production of cosmic strings at the end of inflation, due to the spontaneous breaking of $U(1)_{B-L}$. We will come back to this point in Sec. (3.2). Moreover, the abundance of nonthermally produced gravitinos, controlled by the symmetry-breaking scale, the common mass of the inflaton and $B-L$ Higgs in the true vacuum, and the reheating temperature [43,44],

$$Y_{3/2} \propto \frac{v_{B-L}^2 m_S^2}{T_{\text{RH}}} \,, \tag{14}$$

must be sufficiently low, so that the sum of nonthermal and thermal (cf. section 4) gravitino abundance does not produce a gravitino problem [24–28, 45–47]. Note, however, that the nonthermal gravitino abundance can be suppressed compared to the estimate in Eq. (14), if the massive particle governing the universe during the reheating phase decays sufficiently fast.
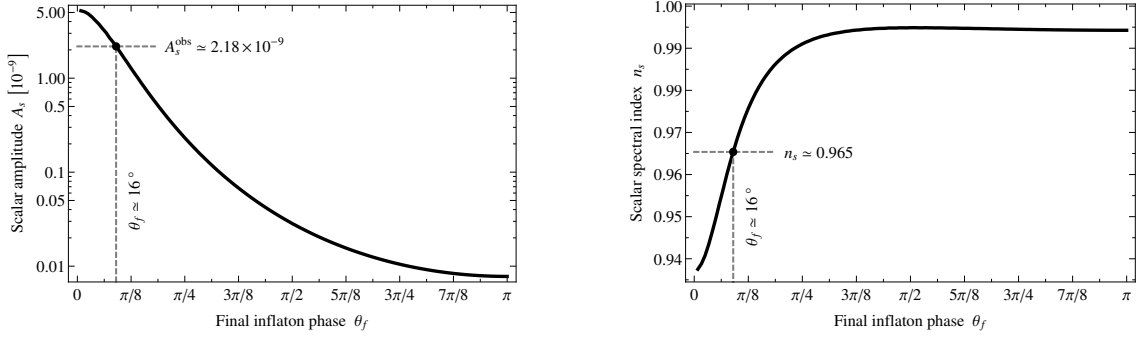
Fig. 3: Amplitude and spectral index of the scalar primordial fluctuations for $\lambda = 4.5 \times 10^{-6}$, $v_{B-L} = 2.9 \times 10^{15}$ GeV and $m_{\widetilde{G}} = 47.5$ TeV. The phase of the endpoint of inflation, θ_f, labels different inflationary trajectories.

Taking all of this together, we find that F-term hybrid inflation is indeed still viable in light of the Planck data, however some tuning is required. Accepting a non-minimal Kähler potential with some tuning in its coefficients as well as in the initial conditions for $|\phi|$, accordance with the Planck data can be achieved for $\theta_f \sim \pi$. Staying with a minimal Kähler potential one has two options to reproduce the experimental data. Either, one tunes the amplitude of the linear term (13) against the CW term (7) in the potential, leading to the situation shown in Fig. 2. In this case small values for n_s can be achieved for $\theta_f \sim 0$, but again tuning of the initial condition for the radial degree $|\phi|$ is necessary to prevent the inflaton from being trapped on the wrong side of the hill-top potential.[4] The second possibility is to allow the linear term to dominate over the CW term, however then the initial phase of ϕ must be tuned because otherwise one lands on a trajectory where inflation does not end, because it 'misses' the minimum generated by the CW term at small $|\phi|$, such that $|\phi|$ always remains larger than the critical value. For a more detailed analysis of the full two-field inflation model, see Ref. [48].

In summary, successful inflation can be achieved but it imposes constraints on the $B-L$ breaking scale and on the coupling λ. In the context of the Froggatt-Nielsen flavour model used to parametrize the Yukawa couplings in Ref. [10], this then constrains the mass of the heaviest of the right-handed neutrinos M_1. In the following, we will thus consider the restricted parameter space

$$
\begin{aligned}
v_{B-L} &= 5 \times 10^{15} \text{ GeV}, \\
10^9 \text{ GeV} &\leq M_1 \leq 3 \times 10^{12} \text{ GeV}, \\
10^{-5} \text{ eV} &\leq \widetilde{m}_1 \leq 1 \text{ eV},
\end{aligned}
\tag{15}
$$

where the variation of the effective light neutrino mass parameter $\widetilde{m}_1$ accounts for the uncertainties of the Froggatt-Nielsen model. The values of v_{B-L} and λ quoted here correspond to the option of choosing $\theta_f = \pi$ and using a non-minimal Kähler potential, cf. Ref. [40]. For a discussion of cosmological $B-L$ breaking involving smaller values for v_{B-L}, cf. Ref. [12].

3 Tachyonic Preheating and Cosmic Strings

The end of hybrid inflation induces a negative squared mass term for the $B-L$ Higgs field σ' in the false vacuum, triggering the $U(1)_{B-L}$ breaking phase transition. The cosmological realization of this phase transition is accompanied by two important nonperturbative processes, tachyonic preheating [33] and the formation of cosmic strings [49].

---

[4]Note that nevertheless, an arbitrary amount of e-folds of inflation can be realized in this setup.

3.1 Tachyonic preheating

The phase transition

Tachyonic preheating is a fast and nonperturbative process triggered by the tachyonic instability in the scalar potential in the direction of the Higgs field. As the inflaton field passes a critical point ϕ_c, the Higgs field σ' acquires a negative effective mass squared $-m_\sigma^2$, with $m_\sigma^2 = \sqrt{2}\lambda v_{B-L}|\dot{\phi}_c|t$ in the linearized equation of motion for σ' close to the instability point ϕ_c. This causes a faster than exponential growth of the quantum fluctuations of the Higgs field σ'_k with wave numbers $|\vec{k}| < m_\sigma$ [50], while the average value of the Higgs field remains zero. Once the amplitude of these fluctuations, $v(t) = \frac{1}{\sqrt{2}}\langle\sigma'^2\rangle = \frac{1}{\sqrt{2}}\langle\sigma'^2(t,\boldsymbol{x})\rangle_{\boldsymbol{x}}^{1/2}$,[5] reaches $\langle\sigma'^2(t_*)\rangle = \mathcal{O}(v_{B-L}^2)$, the curvature of the potential for the homogeneous background field σ' becomes positive and the usual oscillating behaviour of the modes is re-established [33] while $v(t)$ approaches v_{B-L}. A direct consequence of the early phase of exponential growth are high occupation numbers in the low-momentum Higgs modes and hence a semiclassical situation with a large abundance of non-relativistic $B-L$ Higgs bosons.

A further result of this nonperturbative process is the formation of 'bubble'-like inhomogeneities which randomly feature different phases of the complex Higgs field [50, 51]. Their initial size is given by the smallest scale amplified during tachyonic preheating, referred to as k_*^{-1}. These bubbles expand at the speed of light, thereby colliding with each other. This phase of the preheating process is an important source of gravitational waves (GWs), cf. [53], a point to which we will return in Sec. 5. After this very turbulent phase the true Higgs vev is reached in almost the entire volume, with the regimes of false vacuum reduced to topologically stable cosmic strings, cf. Sec. 3.2, separated by the characteristic length scale $k_*^{-1} \approx (\sqrt{2}\lambda v_{B-L}|\dot{\phi}_c|)^{-1/3}$.

Secondary Particle production

The mode equations for the particles coupled to the $B-L$ Higgs field, i.e. for the gauge, Higgs, inflaton and neutrino supermultiplets, feature masses proportional to $v(t)$. The growth of $\langle\sigma'^2\rangle$ during tachyonic preheating thus induces a rapid change of their effective masses. The resulting particle production was studied in Ref. [52], with the results depicted in Fig. 4. Here, for simplicity, an abrupt transition of the inflaton vev to zero is assumed, introducing the parameter $m = m_\sigma(\dot{\phi}_c t \to \phi_c)$.[6] The left panel shows the evolution of $\langle\sigma'^2\rangle$ normalized to the symmetry-breaking scale v_{B-L}, calculated using a lattice simulation (green curve). For comparison, the red curve shows an analytical approximation, $v(t) = \frac{v_{B-L}}{2}\left(1 + \tanh\frac{m(t-t_*)}{2}\right)$. The pink and blue curves depict the number densities of bosonic particles coupled to the Higgs, again calculated using a lattice calculation and an analytical approximation, respectively. The right panel examines the momentum distribution of these bosons (and also of fermions coupled to the Higgs) showing the spectrum of occupation numbers. Again both the numerical and analytical results are shown. We see that just like the Higgs bosons themselves, the particles coupled to it are produced with very low momentum, i.e. non-relativistically.

Based on these results, the energy and number densities for bosons and fermions coupled to the Higgs boson after tachyonic preheating have been estimated as [52][7]

$$\rho_B/\rho_0 \simeq 2 \times 10^{-3}\, g_\sigma\, \lambda\, f(x_1, 1.3)\,, \qquad n_B(x_1) \simeq 1 \times 10^{-3}\, g_\sigma\, m_S^3\, f(x_1, 1.3)/x_1\,,$$
$$\rho_F/\rho_0 \simeq 1.5 \times 10^{-3}\, g_\sigma\, \lambda\, f(x_1, 0.8)\,, \qquad n_F(x_1) \simeq 3.6 \times 10^{-4}\, g_\sigma\, m_S^3\, f(x_1, 0.8)/x_1\,, \tag{16}$$

with $f(x_1, x_2) = (x_1^2 + x_2^2)^{1/2} - x_2$ and $x_1 = m_i/m_S$, where m_i denotes the mass of the respective particle in the true vacuum and g_σ counts its spin and internal degrees of freedom.

---

[5]Here, bold letters indicate 3-vectors.

[6]The effect of the inflaton dynamics on this nonperturbative particle production requires further investigation.

[7]Note that particle production can be significantly enhanced by quantum effects [54], which require further investigation.
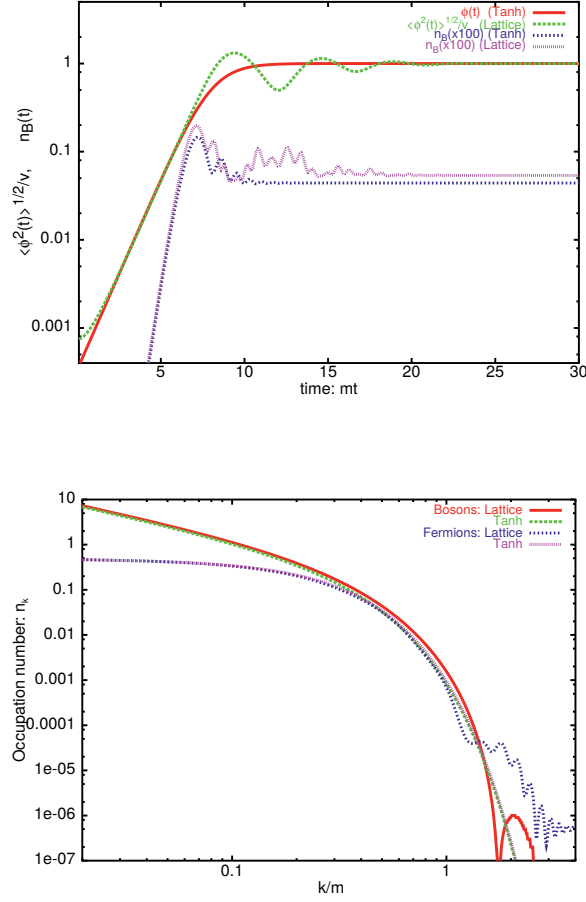
Fig. 4: Numerical and analytical results for particle production during tachyonic preheating, taken from Ref. [52]. **Left panel**: Evolution of the quantum fluctuations of the Higgs field $\phi(t) \equiv \sigma'(t)/\sqrt{2}$, normalized to the symmetry-breaking scale $v \equiv v_{B-L}$, as well as the number density n_B of bosonic particles coupled to it. **Right panel**: Spectrum of occupation numbers for bosonic and fermionic particles coupled to the Higgs.

3.2 Cosmic strings

Due to the non-trivial topology of its vacuum manifold, the Abelian Higgs model underlying the $B-L$ phase transition gives rise to solitonic field configurations, so-called cosmic strings (for a review, see e.g. [55–57]). These cosmic strings are formed during the process of tachyonic preheating and are topologically stable. The evolution of the resulting network is governed by the intersection of the infinite strings, which leads to the formation of closed loops separated from the infinite string, as well as by the energy loss due to the emission of GWs, Higgs and gauge particles. After a relaxation time the network reaches the scaling regime, i.e. the typical length scale of the cosmic string network remains constant relative to the size of the horizon. This implies that a constant fraction of the total energy density is stored in cosmic strings throughout the further evolution of the universe and that there are $\mathcal{O}(1)$ cosmic strings per Hubble volume.

In the scaling regime, the cosmic string network is characterized by the energy per unit length μ. In the Abelian Higgs model, which is based on a field theory featuring a spontaneously broken local

$U(1)$ symmetry, μ is given by [58]

$$\mu = 2\pi B(\beta) v_{B-L}^2, \tag{17}$$

where $\beta = (m_S/m_G)^2 = \lambda/(8g^2)$ is the ratio of the masses of the symmetry-breaking Higgs boson and the gauge boson in the true vacuum, and $B(\beta)$ is a slowly varying function parametrizing the deviation from the Bogomol'nyi bound,

$$B(\beta) \simeq \begin{cases} 1.04\,\beta^{0.195}, & \text{if } 10^{-2} < \beta \ll 1 \\ 2.4\,(\ln\frac{2}{\beta})^{-1}, & \text{if } \beta < 10^{-2} \end{cases}. \tag{18}$$

For the special case of $\beta = 1$ the Bogomol'nyi bound is saturated and $B(1) = 1$ [59].

Further important quantities describing the string network are the cosmic string width, given by m_G^{-1} in the Abelian Higgs model, and the length scale ξ separating two strings. From Sec. 3.1, we know that the characteristic length separating two strings at the time of their formation is

$$\xi = k_*^{-1} = (\sqrt{2}\lambda v_{B-L}|\dot{\phi}_c|)^{-1/3}. \tag{19}$$

This also determines the relaxation time of the cosmic string network, $\tau_{\text{string}} \sim \xi$ [50,60]. Note that in the Nambu-Goto model, an alternative to the Abelian Higgs cosmic string model which assumes infinitely thin cosmic strings, the energy scale μ is an input parameter.

Observational prospects

So far, no experimental evidence for the existence of cosmic strings has been found. However, current and upcoming experiments are starting to seriously probe the cosmologically interesting regions of the parameter space. First, cosmic strings give rise to anisotropies in the CMB temperature map. They distort the surface of last scattering of the CMB photons, leaving an imprint on the spectrum observable today. Since the CMB photons observable today stem from roughly 10^5 Hubble patches during recombination, these observations are mainly sensitive to the effect of long (Hubble-sized) strings at recombination and not to small cosmic string loops. In contrast to the perturbations due to inflation, these anisotropies are not phase correlated across distant Hubble patches and hence the resulting multipole spectrum of the two-point correlation function is suppressed at large scales and moreover does not show the oscillations characteristic to inflation. Moreover, whereas the primordial power spectrum due to inflation is (nearly) scale-invariant, the anisotropies on the last scattering surface due to cosmic strings are governed by a characteristic scale. The resulting spectrum thus features a single broad peak associated with this scale. Due to the re-scattering of a fraction of the CMB photons at reionisation, the CMB spectrum is, to a lesser extent, also sensitive to the long cosmic strings present at reionisation. This leads to a second, smaller peak in the spectrum, in particular visible in the power spectrum of the B-mode polarization, see e.g. [61] for a recent analysis. The fraction of the amplitude of the scalar power spectrum due to a possible cosmic string contribution to the CMB temperature anisotropies is conventionally measured at the multipole $l = 10$ and is referred to as f_{10}. The Planck data implies that f_{10} can at most be a few percent, $f_{10} < 2.8\%$ [38].

Second, the gravitational field of cosmic strings gives rise to weak and strong lensing effects of (CMB) photons on their way from the surface of last scattering or from an astrophysical source to us. The non-observation of such effects puts a bound on the string tension μ. Again, this effect is mainly sensitive to long (Hubble-sized) strings.

Third, the energy emitted by cosmic strings in the scaling regime is at least partly emitted in form of GWs. Due to their extremely weak coupling, these can then propagate freely through the universe and are therefore in principle detectable today. We will come back to the resulting GW background and the discovery potential of current and upcoming GW experiments in detail in Sec. 5.

Finally, the Abelian Higgs cosmic string model entails the emission of massive radiation from cosmic strings, i.e. the emission of the Higgs and gauge particles whose field configurations form the

string. If this mechanism is still active at late times it could yield ultra-high-energetic cosmic rays and GeV-scale γ-rays, which have not been observed. This too, can be translated into a (model-dependent) bound on μ [62–66].

Currently the most stringent and model-independent bound on the cosmic string tension comes from CMB observations, $G\mu < 3.2 \times 10^{-7}$ [38], and we shall mainly employ this in the following.

Numerical simulations and theoretical uncertainties

A quantitative understanding of the formation of cosmic strings, the dynamics of the cosmic string network and the energy loss mechanism during the scaling regime requires lattice simulations. Performing these is extremely challenging due to the huge range of scales involved in the problem [56]: the width of the string remains constant while the scales of the network are blown up as the universe expands. Or, in comoving coordinates, the comoving width of the string shrinks, until it becomes comparable with the lattice spacing and the simulation loses its validity. There have been different approaches to tackle this problem. Simulations based on solving the field equations for the Abelian Higgs (AH) model set the comoving width to a finite constant before it comes too close to the lattice spacing [60, 67, 68]. Simulations based on the Nambu-Goto (NG) string model assume cosmic strings to be infinitely thin, i.e. strictly one-dimensional objects, throughout the simulation [69–72]. The outcome of simulations based on these two models is dramatically different. The AH simulations show the formation of large, Hubble-sized structures which lose their energy predominantly by emitting massive radiation, i.e. particles of the Higgs and gauge fields forming the string configuration. The NG simulations on the other hand display the formation of small loops, which lose their energy into GWs. The size of these loops is thought to be controlled by gravitational backreaction, but is as yet undetermined [56]. Concerning the network of long strings, both simulations, however, yield a similar result [56]. Which of these two simulations methods is closer to reality is currently an open question.

In the following, we will adopt the following hypothesis: For early times, while the comoving cosmic string width is large compared to the lattice spacing, the AH simulation describes the $U(1)$ phase transition very well. We will thus use the results from these simulations when discussing the formation and early evolution of cosmic strings. For late times, the AH simulations become questionable and the NG approximations of infinitely thin strings appears reasonable. Hence for late times, in particular when discussing possible GW signatures from cosmic strings, cf. Sec. 5, we shall discuss both the AH as well as the NG results.

4 Reheating

Tachyonic preheating nonperturbatively generates a large abundance of non-relativistic $B{-}L$ Higgs bosons as well as, to a much lesser extent, non-relativistic abundances of the particles coupled to the Higgs boson, cf. Sec. 3.1. Among these are the particles of the $B{-}L$ gauge supermultiplet, which decay quickly due to their comparatively strong gauge interactions. This sets the initial conditions for the following slow, perturbative reheating process, depicted by the solid arrows in the left panel of Fig. 5: The particles from the symmetry-breaking sector decay into particles of the N_1 supermultiplet. These (s)neutrinos, just as the (s)neutrinos produced through gauge particle decays and tachyonic preheating as well as thermally produced (s)neutrinos, decay into MSSM particles, thereby generating the entropy of the thermal bath as well as a lepton asymmetry [73]. Finally, the thermal bath produces a thermal gravitino abundance, which will turn out to be in the right ball-park to yield the observed dark matter abundance.

The main tool to obtain a time-resolved description of this reheating process are Boltzmann equations, which describe the evolution of the phase space densities of the various particles species due to decay and scattering processes in an expanding universe. After briefly introducing the formalism of Boltzmann equations in Sec. 4.1, we will turn to the implications for leptogenesis and dark matter production in Sec. 4.2. The results presented here are based on the analyses of Refs. [10–12].
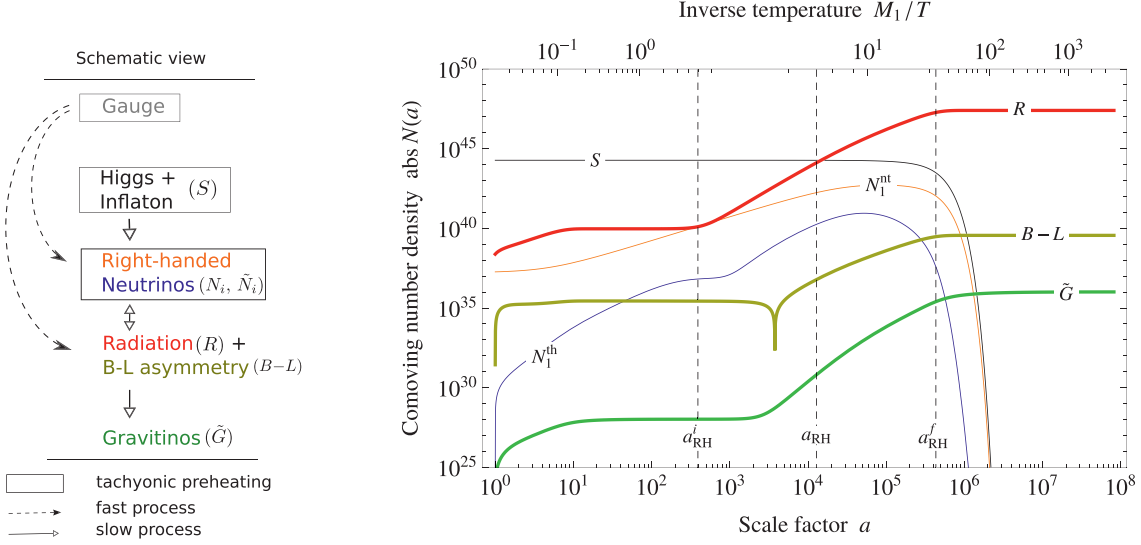
Fig. 5: Evolution of the comoving number densities during the reheating process. **Left panel**: schematic overview, distinguishing production via tachyonic preheating, fast decay processes of the $B-L$ gauge sector and slow processes described by Boltzmann equations. **Right panel**: Comoving number densities of the particles of the $B-L$ Higgs sector (S), the thermal and nonthermal (s)neutrinos (N_1^{th}, N_1^{nt}), the MSSM radiation (R), the gravitinos ($\widetilde{G}$) and the $B-L$ asymmetry ($B-L$). Obtained by solving the Boltzmann equations for $v_{B-L} = 5 \times 10^{15}$ GeV, $M_1 = 5.4 \times 10^{10}$ GeV, $\widetilde{m}_1 = 4.0 \times 10^{-2}$ eV, $m_{\widetilde{G}} = 100$ GeV and $m_{\tilde{g}} = 1$ TeV. From Ref. [10].

4.1 Boltzmann equations

The evolution of the phase space density $f_X(t,p)$ of a particle species X is determined by a coupled set of Boltzmann equations,

$$E\left(\frac{\partial}{\partial t} - Hp\frac{\partial}{\partial p}\right) f_X(t,p) = \sum_{i'j'..}\sum_{ij..} C_X(Xi'j'.. \leftrightarrow ij..)\,, \tag{20}$$

augmented by the Friedmann equation, which governs the evolution of the scale factor. The left-hand side of Eq. (20) describes the evolution of the phase space density in an expanding Friedman-Robertson-Walker (FRW) universe whereas the collision operators C_X on the right-hand side account for all relevant scattering, decay and inverse decay processes involving the particle X. The set of Boltzmann equations we have to solve here is determined by the allowed interactions of the underlying particle physics model, cf. solid blue arrows in the left panel of Fig. 5.

From the phase space density $f_X(t,p)$ one directly obtains the comoving number density $N_X(t)$, i.e. the number of X particles in a volume $(a/\text{GeV})^3$, and the energy density $\rho_X(t)$ by integrating over momentum space,

$$N_X(t) = \left(\frac{a(t)}{\text{GeV}}\right)^3 n_X = \left(\frac{a(t)}{\text{GeV}}\right)^3 g_X \int \frac{d^3p}{(2\pi)^3}\, f_X(t,p)\,,$$
$$\rho_X(t) = g_X \int \frac{d^3p}{(2\pi)^3}\, E_X(p)\, f_X(t,p)\,, \tag{21}$$

with a denoting the scale factor. A rescaling of a leaves the physical number density n_X invariant. For convenience, we will thus set $a_{\text{PH}} \equiv 1$ at the end of preheating. In the following, decay rates Γ, comoving number densities N and energy densities ρ will sometimes appear with upper and lower indices. In this case, the lower index refers to the particle species under consideration, while the upper index refers to its origin, e.g. its parent particle or 'PH' for preheating.

4.2 Outcome of the reheating process

Solving the Boltzmann equations with the initial conditions given by tachyonic preheating and the successive decay of the $B-L$ gauge bosons yields a time-resolved picture of the evolution of all particle species. In the right panel of Fig. 5, we show an overview of the resulting comoving number densities for a representative parameter point.

A two-stage reheating process
After the end of preheating, the lion's share of the energy is stored in non-relativistic $B-L$ Higgs bosons. Assuming a hierarchical spectrum of heavy Majorana neutrinos, these decay exclusively into heavy, typically relativistic (s)neutrinos of the first generation, thereby forming the main part of the right-handed (s)neutrino population. The decay of these (s)neutrinos then generates a thermal bath of MSSM particles. The process of reheating is hence governed by the interplay of two time-scales, the vacuum decay rate of the non-relativistic Higgs bosons Γ_S^0 and the effective decay rate of the neutrinos produced in the Higgs boson decays $\Gamma_{N_1}^S$. The latter differs from the zero-temperature decay rate $\Gamma_{N_1}^0$ due to the time-dilation of the relativistic neutrinos,

$$
\Gamma_S^0 = \frac{1}{32\pi} \left(\frac{M_1}{v_{B-L}} \right)^2 m_S \left(1 - 4\frac{M_1^2}{m_S^2} \right)^{1/2} ,
$$

$$
\Gamma_{N_1}^S := \Gamma_{N_1}^S(a_{\mathrm{RH}}) = \gamma^{-1}(a_{\mathrm{RH}}) \, \Gamma_{N_1}^0 \quad \text{with} \quad \gamma^{-1}(a) = \left\langle \frac{M_1}{E_{N_1}} \right\rangle_a^{(S)} , \quad \Gamma_{N_1}^0 = \frac{1}{4\pi} \frac{\widetilde{m}_1 M_1^2}{v_{\mathrm{EW}}^2} .
$$

(22)

In most of the viable parameter space, we find $\Gamma_S^0 < \Gamma_{N_1}^S$. In this case, Γ_S^0 determines the overall time-scale of the reheating process. On the contrary a_{RH}, defined by $H(a_{\mathrm{RH}}) = \Gamma_{N_1}^S(a_{\mathrm{RH}})$, marks a characteristic point in the middle of the reheating process, which will be in particular relevant for determining the reheating temperature. Once the Higgs bosons decay into neutrinos, these decay nearly instantaneously into MSSM particles, so that the era of Higgs domination is directly followed by the radiation dominated epoch. On the other hand, if $\Gamma_S^0 > \Gamma_{N_1}^S$, the effective neutrino decay rate governs the time-scale of reheating. The energy density is then successively governed by non-relativistic Higgs bosons, relativistic nonthermal neutrinos and finally relativistic thermal MSSM particles.

Solving the Boltzmann equations allows us to determine the temperature of the thermal bath throughout the reheating process. As a consequence, the 'reheating temperature' is no longer a cosmological input parameter, but is rather determined by the parameters of the $B-L$ Higgs and neutrino sector. In Fig. 6 we show the resulting evolution of the temperature. A remarkable feature is the epoch of nearly constant temperature during the main part of the reheating process, which arises because the entropy production from the neutrino decays just compensates the expansion of the universe. A typical value for this plateau is given by $T_{\mathrm{RH}}^N \equiv T(a_{\mathrm{RH}})$, with a_{RH} as defined above. The dashed vertical lines labeled a_{RH}^i and a_{RH}^f in Figs. 5 and 6 mark the beginning and the end of the reheating process, defined as the period when the effective production rate of MSSM particles exceeds the Hubble rate.

Thermal and nonthermal leptogenesis
The decays of the thermally and nonthermally produced neutrinos give rise to a thermal and a nonthermal $B-L$ asymmetry, as depicted in Fig. 7. The nonthermal lepton asymmetry receives a first contribution from the decay of the heavy (s)neutrinos of the second and third generation. To clearly distinguish this contribution from the main contribution arising due to the decay of the first-generation (s)neutrinos, we have assigned opposite signs to the parameters $\epsilon_{2,3}$ and ϵ_1 quantifying the CP asymmetry in decays of the respective neutrino generations. This entails the change of sign visible at $a \simeq 4.6 \times 10^3$ in Fig. 7, when the decay of N_1^S neutrinos becomes efficient and the main part of the nonthermal asymmetry is produced. Wash-out effects are negligibly small throughout this process and hence, once the production of the nonthermal asymmetry becomes inefficient, the asymmetry freezes out.
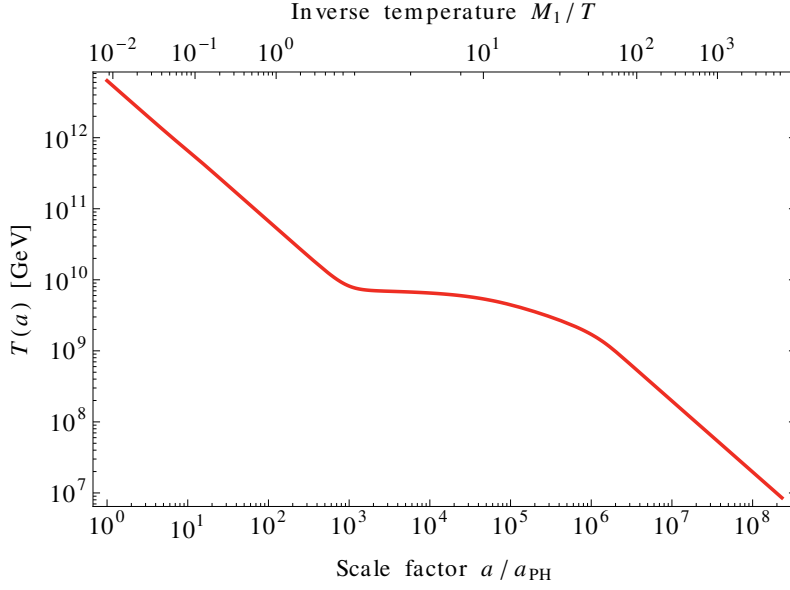
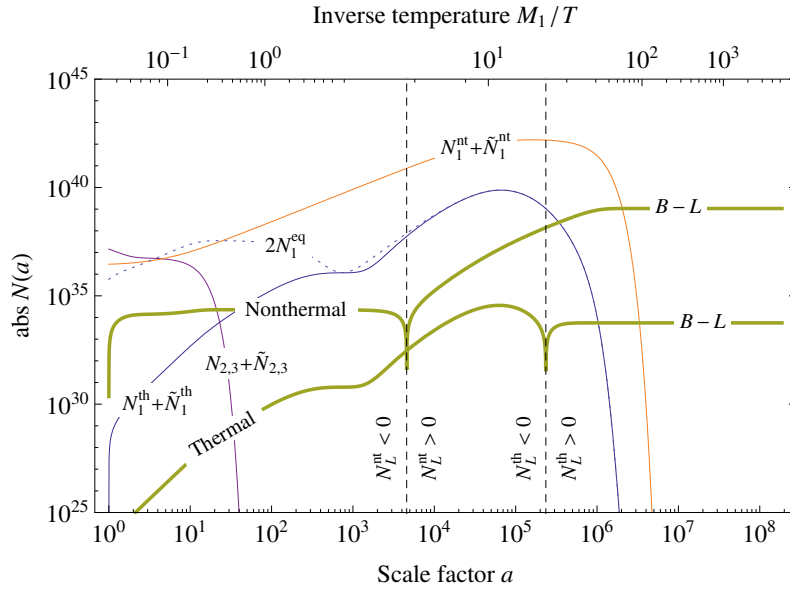**Fig. 6:** Temperature of the thermal bath for the same parameter values as in Fig. 5. From Ref. [10].

Fig. 7: Comoving number densities for the nonthermal (N_L^{nt}) and thermal (N_L^{th}) contributions to the total lepton asymmetry as well as all (s)neutrino species ($N_1^{\text{nt}} + \tilde{N}_1^{\text{nt}}$, $N_1^{\text{th}} + \tilde{N}_1^{\text{th}}$, $2N_1^{\text{eq}}$ for comparison and $N_{2,3} + \tilde{N}_{2,3}$) as functions of the scale factor a. The vertical lines mark the changes in the signs of the two components of the lepton asymmetry. From Ref. [10].

The production of the thermal asymmetry is driven by the deviation of the thermal (s)neutrino abundance from the equilibrium value. This leads to an initially negative asymmetry with a rapidly increasing absolute value. This increase slows down as the thermal (s)neutrino abundance approaches the equilibrium value. At around $a \simeq 6.3 \times 10^4$ wash-out processes start to play a role, leading to a decrease of the asymmetry. The situation rapidly changes when the thermal (s)neutrino abundance overshoots the equilibrium abundance towards the end of the reheating process. This generates an asymmetry with an opposite sign, which overcompensates the asymmetry generated so far. Shortly after, both the wash-out rate and production rate drop significantly below the Hubble rate and the asymmetry freezes out.

The final values of thermal and nonthermal asymmetry as depicted in Fig. 7 allow us to infer the present baryon asymmetry η_B as well as its composition in terms of a nonthermal ($\eta_B^{\rm nt}$) and a thermal ($\eta_B^{\rm th}$) contribution,

$$\eta_B = \frac{n_B^0}{n_\gamma^0} = \eta_B^{\rm nt} + \eta_B^{\rm th}, \quad \eta_B^{\rm nt,th} = C_{\rm sph} \frac{g_{*,s}^0}{g_{*,s}^{\rm RH}} \left. \frac{N_L^{\rm nt,th}}{N_\gamma} \right|_{a_f}. \tag{23}$$

Here, $C_{\rm sph} = 8/23$ denotes the sphaleron conversion factor, $g_{*,s}^{\rm RH} = 915/4$ and $g_{*,s}^0 = 43/11$ are the effective numbers of relativistic degrees of freedom in the MSSM that enter the entropy density s of the thermal bath in the high- and low-temperature regime, respectively, $N_L^{\rm nt,th}$ refers to the comoving number density for the nonthermal and thermal contribution to the lepton asymmetry and $N_\gamma = g_\gamma/g_{*,n} N_r$ is the comoving number density of photons. For our parameter example we find

$$\eta_B \simeq 3.7 \times 10^{-9}, \quad \eta_B^{\rm nt} \simeq 3.7 \times 10^{-9}, \quad \eta_B^{\rm th} \simeq 1.9 \times 10^{-14}. \tag{24}$$

Note that to obtain these values, we have set the CP-violation parameter in the first generation neutrino decays ϵ_1 to the maximally allowed value, see Ref. [10]. Hence η_B in Eq. (24) yields an upper bound on the baryon asymmetry produced in this setup and is thus perfectly compatible with the observed value, $\eta_B^{\rm obs} \simeq 6.2 \times 10^{-10}$ [74]. In fact, the Froggatt-Nielsen model typically predicts a value for ϵ_1 that is smaller than the maximal possible value by roughly a factor of $\mathcal{O}(10)$, cf. Ref. [75], implying excellent agreement between prediction and observation for this parameter example, $\eta_B \simeq \eta_B^{\rm obs}$.

Gravitino or neutralino dark matter

The thermal bath produced in the decays of the heavy neutrinos gives rise to a thermal gravitino abundance, which can, depending on the underlying low-energy supersymmetry mass spectrum, be either directly or via its decay products linked to today's dark matter abundance. In the former case, we assume the gravitino to be the lightest supersymmetric particle (LSP), as arises for instance in gaugino-mediated supersymmetry breaking. In this case, we can deduce today's gravitino dark matter abundance $\Omega_{\widetilde{G}} h^2$ from the final value of the comoving gravitino abundance $N_{\widetilde{G}}$:

$$\Omega_{\widetilde{G}} h^2 = \frac{\rho_{\widetilde{G}}^0}{\rho_c/h^2} = \frac{m_{\widetilde{G}} \, n_\gamma^0}{\rho_c/h^2} \frac{g_{*,s}^0}{g_{*,s}^{\rm RH}} \left. \frac{N_{\widetilde{G}}}{N_\gamma} \right|_{a_f}, \tag{25}$$

where $\rho_c = 3H^2/(8\pi G) = 1.05 \times 10^{-5} \, h^2 \, {\rm GeV\, cm^{-3}}$ denotes the critical energy density of the universe, h the Hubble rate in the units $H = h \times 100 \, {\rm km\, s^{-1}\, Mpc^{-1}}$ and $n_\gamma^0 = 410 \, {\rm cm^{-3}}$ the present number density of the CMB photons. Due to the high temperatures reached in this setup, we do not expect a significant contribution from nonthermal gravitino production. For the parameter example shown in Fig. 5 we find $\Omega_{\widetilde{G}} h^2 \simeq 0.11$, matching the observed amount of dark matter $\Omega_{\rm DM}^{\rm obs} h^2 \simeq 0.11$ [74][8]. Note that in the choice of this parameter example $M_1 = 5.4 \times 10^{11}$ GeV was adjusted to obtain this result. Performing a parameter scan over $\widetilde{m}_1$ and $m_{\widetilde{G}}$, thereby adjusting M_1 to achieve the correct gravitino

---

[8]The recently published Planck data yields a slightly larger value, $\Omega_{\rm DM}^{\rm obs} h^2 = 0.12$ [76]. The effect of this change on the work presented here is marginal, and in the following we will stay with the value quoted above.
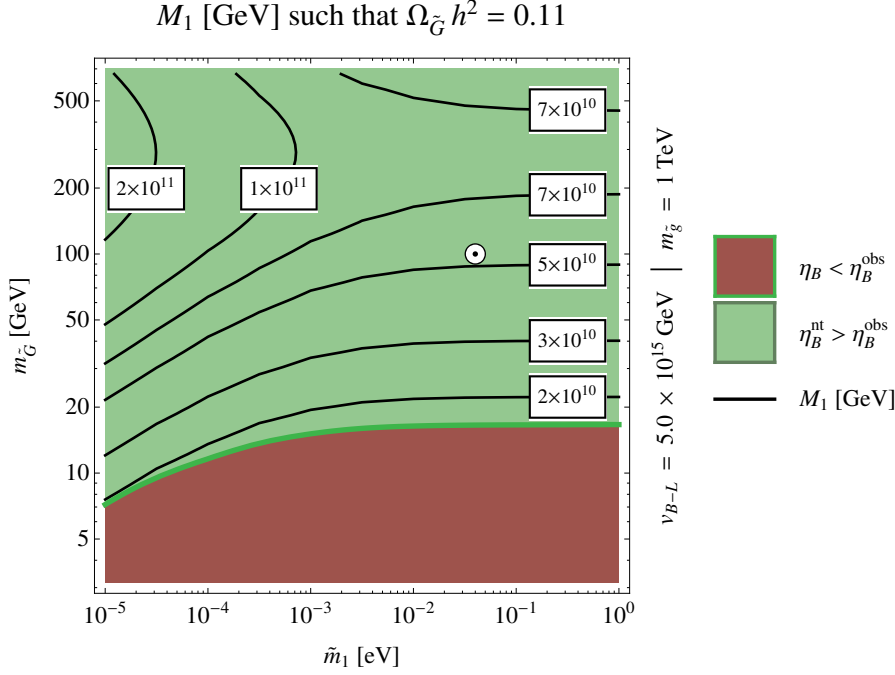
Fig. 8: Contour plots of the heavy neutrino mass M_1 as a function of the effective neutrino mass $\widetilde{m}_1$ and the gravitino mass $m_{\widetilde{G}}$ such that the relic density of dark matter is accounted for by gravitinos. In the red region the lepton asymmetry generated by leptogenesis is smaller than the observed one, providing a lower bound on the gravitino mass dependent on $\widetilde{m}_1$. The small white circle marks the position of the parameter point discussed in Figs. 5 - 7. From Ref. [10].

dark matter abundance, yields the viable parameter space as depicted in Fig. 8. The red shaded region is excluded due to an insufficient production of baryon asymmetry, whereas in the green shaded region we produce a sufficient amount of baryon asymmetry (mainly nonthermally) as well as the correct dark matter abundance. In this region, the reheating temperature ranges from $\mathcal{O}(10^8)$ to $\mathcal{O}(10^{10})$ GeV.

As can be seen from Fig. 8, requiring successful leptogenesis as well as the correct dark matter abundance thus yields a lower bound on the gravitino mass $m_{\widetilde{G}}$ in terms of the effective neutrino mass parameter $\widetilde{m}_1$,

$$m_{\widetilde{G}} \geq 16 \, \text{GeV} \left(\frac{m_{\tilde{g}}}{1 \, \text{TeV}} \right)^2 \left(\frac{\widetilde{m}_1}{10^{-3} \, \text{eV}} \right)^{0.25-c}, \quad c = \begin{cases} -0.01 & \text{for } \widetilde{m}_1 \lesssim 10^{-3} \, \text{eV} \\ 0.21 & \text{for } \widetilde{m}_1 \gtrsim 10^{-3} \, \text{eV} \end{cases}. \quad (26)$$

with the value of the exponent c determined by numerically solving the Boltzmann equations. Eq. (26) links a parameter of the neutrino mass sector related to $B-L$ breaking to a parameter involved in low-energy supersymmetry breaking. Physically, this bound can be understood as follows. For gravitino masses below $\mathcal{O}(10)$ GeV, a reheating temperature $T_{\text{RH}}^N \lesssim \mathcal{O}(10^8 - 10^9)$ GeV is required to avoid overproduction of gravitinos. According to our reheating mechanism such low reheating temperatures are associated with relatively small values of the neutrino mass, $M_1 \lesssim \mathcal{O}(10^{10})$ GeV. The low temperature and low mass then entail a small abundance of (s)neutrinos at the time the asymmetry is generated and a small CP parameter ϵ_1. Both effects combine and result in an insufficient lepton asymmetry, rendering dark matter made of gravitinos with a mass below $\mathcal{O}(10)$ GeV inconsistent with leptogenesis.

Alternatively, as discussed in Ref. [32], we can assume a hierarchical supersymmetric mass spectrum with the gravitino as the heaviest particle and a neutralino with mass m_χ as the LSP,

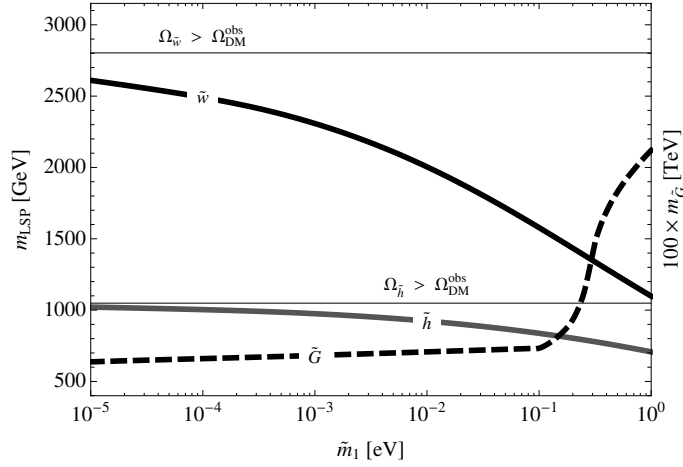$$m_\chi \ll m_{\text{squark, slepton}} \ll m_{\widetilde{G}}, \quad (27)$$

Fig. 9: Upper bounds on wino ($\widetilde{w}$) and higgsino ($\widetilde{h}$) LSP masses imposed by successful leptogenesis as well as absolute lower bound on the gravitino mass according to BBN as functions of the effective neutrino mass $\widetilde{m}_1$. Wino masses larger than 2.8 TeV and higgsino masses larger than 1.0 TeV result in thermal overproduction of DM. From Ref. [32].

as is found, for instance, in Refs. [77–79]. Due to this hierarchy the LSP is typically a 'pure' gaugino or higgsino [80]. Generically, the thermal abundance of a bino LSP is too large. We therefore focus on the possibility of a wino or higgsino LSP[9]. There are then two relevant production channels for neutralino dark matter: thermal production, accompanied by the standard thermal freeze-out mechanism for weakly interacting massive particles (WIMPs), and nonthermal production, as a decay product of the gravitinos produced during the reheating process. In the parameter regime of interest, the resulting thermal and nonthermal abundances can be estimated as Ω_χ^{th} [83–85] and $\Omega_\chi^{\widetilde{G}}$, respectively:

$$
\begin{aligned}
\Omega_\chi^{\text{th}} h^2 &= c_\chi \left(\frac{m_\chi}{1\,\text{TeV}} \right)^2 , \qquad c_{\widetilde{w}} = 0.014 , \quad c_{\widetilde{h}} = 0.10 \\
\Omega_\chi^{\widetilde{G}} h^2 &= \left(\frac{m_\chi}{m_{\widetilde{G}}} \right) \Omega_{\widetilde{G}} h^2 \simeq 2.7 \times 10^{-2} \left(\frac{m_\chi}{100\,\text{GeV}} \right) \left(\frac{T_{\text{RH}}^N(M_1, \widetilde{m}_1)}{10^{10}\,\text{GeV}} \right) .
\end{aligned}
\tag{28}
$$

Here $c_{\widetilde{w}}$ and $c_{\widetilde{h}}$ apply to the wino and higgsino case, respectively, and $\Omega_{\widetilde{G}}$ refers to the 'would-be' gravitino abundance today if the gravitinos were stable. Requiring the total neutralino LSP abundance to match the observed dark matter abundance constrains the reheating temperature, depending on the value of the neutralino LSP mass m_χ. Additionally taking into account the bounds from successful leptogenesis and big bang nucleosynthesis (BBN) on the reheating temperature, we find upper bounds on the neutralino LSP mass and an absolute lower bound on the gravitino mass (for all neutralino LSP masses) depending on the value of $\widetilde{m}_1$, as depicted in Fig. 9. As in the gravitino LSP case, we thus find relations between the neutrino and superparticle mass spectrum, induced by the key role of the reheating temperature in the efficiency of both leptogenesis and thermal gravitino production.

5 Gravitational Waves

So far, we have discussed the birth of the hot early universe in the MSM as well as indirect probes of this mechanism in terms of the resulting neutrino and dark matter properties. We now turn to the possibility of directly probing such early universe physics by measuring the gravitational wave (GW) background

---

[9]Recently it has been shown that wino DM is strongly constrained by indirect searches using the H.E.S.S. and Fermi gamma-ray telescopes [81, 82].

[86]. GWs are generated by nonspherical, inhomogeneous strong gravitational field dynamics, decouple immediately from their source and to very good approximation propagate freely ever since. Hence, GWs can carry information on the very early universe.

5.1 Cosmic gravitational wave background

Gravitational waves are tensor perturbations of the homogeneous background metric. In a flat FRW background, these perturbations can be parametrized as [87]

$$ds^2 = a^2(\tau)\,(\eta_{\mu\nu} + h_{\mu\nu})dx^\mu dx^\nu\,. \tag{29}$$

Here $\eta_{\mu\nu} = \mathrm{diag}(-1,1,1,1)$ and $h_{\mu\nu}$ denotes the tensor perturbation. x^μ are conformal coordinates with x^i, $i = 1..3$, denoting the comoving spatial coordinates and $\tau = x^0$ the conformal time. These are related to the physical coordinates and the cosmic time as $\boldsymbol{x}_{\mathrm{phys}} = a(\tau)\,\boldsymbol{x}$ and $dt = a(\tau)\,d\tau$, respectively.

The tensor perturbation evolves dynamically according to the Einstein equation. In the vacuum, $h_{\mu\nu}$ contains two physical degrees of freedom. A convenient gauge choice is the transverse traceless (TT) gauge, i.e. $h^{0\mu} = 0$, $h_i^i = 0$ and $\partial^j h_{ij} = 0$. In the weak field approximation, the linearized Einstein equation in momentum space yields the following mode equation for the tensor perturbation around the FRW background in the TT gauge,

$$\tilde{h}_{ij}^{''}(\boldsymbol{k},\tau) + \left(k^2 - \frac{a^{''}}{a}\right)\tilde{h}_{ij}(\boldsymbol{k},\tau) = 16\pi\,G\,a\,\Pi_{ij}(\boldsymbol{k},\tau)\,, \tag{30}$$

describing the generation and propagation of GWs. Here $\tilde{h}_{ij} = ah_{ij}$, Π_{ij} denotes the Fourier transform of the TT part of the anisotropic stress-energy tensor $T_{\mu\nu}$ of the source, $k = |\boldsymbol{k}|$, $\boldsymbol{k}$ is the comoving wave number, related to the physical wave number through $\boldsymbol{k}_{\mathrm{phys}} = \boldsymbol{k}/a$, and the prime denotes the derivative with respect to conformal time.

A useful plane wave expansion for freely propagating GWs is given by

$$h_{ij}(\boldsymbol{x},\tau) = \sum_{P=+,\times}\int_{-\infty}^{+\infty}\frac{dk}{2\pi}\int d^2\hat{\boldsymbol{k}}\,h_P(\boldsymbol{k})\,T_k(\tau)\,e_{ij}^P(\hat{k})\,e^{-ik(\tau-\hat{\boldsymbol{k}}\boldsymbol{x})}\,, \tag{31}$$

where $\hat{\boldsymbol{k}} = \boldsymbol{k}/k$, $P = +,\times$ labels the two possible polarization states of a GW in the TT gauge and $e_{ij}^{+,\times}$ are the two corresponding polarization tensors satisfying the normalization condition $e_{ij}^P e^{ij\,Q} = 2\delta^{PQ}$. $h_P(\boldsymbol{k})$ denote the coefficients of the expansion after factorizing out the red-shift due to the expansion of the universe, with the latter captured in the so-called transfer function $T_k(\tau)$.

An analytical expression for T_k can be obtained by studying the source-free version of Eq. (30). The resulting mode equation can be easily solved, revealing that the amplitude $h_{ij}(k)$ of a given mode remains constant in the super-horizon regime, $k \ll aH$, while it decreases as $1/a$ inside the horizon, i.e. for $k \gg aH$. Identifying the transfer function T_k as $T_k(\tau_*,\tau) = h_{ij}^E(\boldsymbol{k},\tau)/h_{ij}^E(\boldsymbol{k},\tau_*)$, with $h_{ij}^E(\boldsymbol{k},\tau)$ denoting the envelope of the oscillating function $h_{ij}(\boldsymbol{k},\tau)$, we can employ the approximation[10] (see e.g. [88])

$$T_k(\tau_*,\tau_0) \approx \frac{a(\tau_*)}{a(\tau_0)} \qquad \text{with } \tau_* = \begin{cases} \tau_i \text{ for sub-horizon sources} \\ \tau_k \text{ for super-horizon sources} \end{cases}. \tag{32}$$

Here, τ_i marks the time when the GW was generated and τ_k denotes the time when a given mode with wave number k entered the horizon, $k = a(\tau_k)\,H(\tau_k)$. In Eq. (32), we assume for super-horizon sources

---

[10]In Sec. 4, we set $a_{\mathrm{PH}} = 1$. Another convention used frequently is $a_0 = 1$, with a_0 referring to the value of the scale factor today. In this section, we explicitly keep a_0 without specifying a convention. In the end, the dependence on a_0 must drop out of the observables independent of the choice of convention.

that the amplitude is constant until $\tau = \tau_k$ and then drops as $1/a$ immediately afterwards. The actual solution to the mode equation yields corrections to both of these assumptions. However, as a numerical check reveals, these two effects roughly compensate each other so that Eq. (32) reproduces the full result very well. For super-horizon sources we will use the more compact notation $T_k(\tau) = T_k(\tau_k, \tau)$ in the following.

The GW background is a superposition of GWs propagating with all frequencies in all directions. An important observable characterizing the GW background is the ensemble average of the energy density [87], which is expected to be isotropic,

$$\rho_{\text{GW}}(\tau) = \frac{1}{32\pi G} \left\langle \dot{h}_{ij}(\boldsymbol{x}, \tau) \, \dot{h}^{ij}(\boldsymbol{x}, \tau) \right\rangle = \int_{-\infty}^{\infty} d\ln k \, \frac{\partial \rho_{\text{GW}}(k, \tau)}{\partial \ln k} \, , \tag{33}$$

with the angular brackets denoting the ensemble average and the dot referring to the derivative with respect to cosmic time. Alternatively, one uses the ratio of the differential energy density to the critical density,

$$\Omega_{\text{GW}}(k, \tau) = \frac{1}{\rho_c} \frac{\partial \rho_{\text{GW}}(k, \tau)}{\partial \ln k} \, . \tag{34}$$

In the model considered in this paper, the energy density has a part of quantum origin and a part of classical origin, $\rho_{\text{GW}}(\tau) = \rho_{\text{GW}}^{\text{qu}}(\tau) + \rho_{\text{GW}}^{\text{cl}}(\tau)$. The former part is due to inflation and is therefore stochastic, whereas the latter part is determined by the contributions to the stress energy tensor from cosmic strings and from tachyonic preheating, $\rho_{\text{GW}}^{\text{cl}}(\tau) = \rho_{\text{GW}}^{\text{CS}} + \rho_{\text{GW}}^{\text{PH}}(\tau)$.

For a stochastic GW background the Fourier modes $h_A(\boldsymbol{k})$ are random variables and their ensemble average of their two-point function is determined by a time-independent spectral density $S_h(k)$ [87],

$$\left\langle h_P(\boldsymbol{k}) \, h_Q^*(\boldsymbol{k}') \right\rangle = 2\pi \, \delta(k - k') \, \frac{1}{4\pi} \delta^{(2)}(\hat{\boldsymbol{k}} - \hat{\boldsymbol{k}}') \, \delta_{PQ} \, \frac{1}{2} \, S_h(k) \, . \tag{35}$$

This relation reflects the fact that different modes are uncorrelated and that the background is isotropic. Exploiting Eqs. (31)–(35), we can express the differential energy density due to a stochastic source in terms of the spectral density as

$$\frac{\partial \rho_{\text{GW}}(k, \tau)}{\partial \ln k} = \frac{a^2(\tau_*)}{16\pi^2 \, G \, a^4(\tau)} \, k^3 \, S_h(k) \, . \tag{36}$$

The classical contribution to the GW energy density is obtained by integrating Eq. (30) from the initial time τ_i of GW production until today,

$$h_{ij}(\boldsymbol{k}, \tau) = 16\pi G \, \frac{1}{a(\tau)} \int_{\tau_i}^{\tau} d\tau' \, a(\tau') \, \mathcal{G}(k, \tau, \tau') \, \Pi_{ij}(\boldsymbol{k}, \tau') \, , \tag{37}$$

where $\mathcal{G}(k, \tau, \tau')$ is the retarded Green's function of the differential operator on the left-hand side of Eq. (30). For sub-horizon modes, i.e. $k\tau \gg 1$, one has $\mathcal{G}(k, \tau, \tau') = \sin(k(\tau - \tau'))/k$. With this, one can evaluate the ensemble average $\langle \dot{h}^2 \rangle$ in terms of $\langle \Pi^2 \rangle$ by calculating the derivative of Eq. (37) on sub-horizon scales. Assuming translation invariance and isotropy of the source,

$$\left\langle \Pi_{ij}(\boldsymbol{k}, \tau) \Pi^{ij}(\boldsymbol{k}', \tau') \right\rangle = (2\pi)^3 \, \Pi^2(k, \tau, \tau') \, \delta(\boldsymbol{k} + \boldsymbol{k}') \, , \tag{38}$$

the resulting differential energy density simplifies to

$$\frac{\partial \rho_{\text{GW}}(k, \tau)}{\partial \ln k} = \frac{2G}{\pi} \frac{k^3}{a^4(\tau)} \int_{\tau_i}^{\tau} d\tau_1 \int_{\tau_i}^{\tau} d\tau_2 \, a(\tau_1) \, a(\tau_2) \, \cos(k(\tau_1 - \tau_2)) \, \Pi^2(k, \tau_1, \tau_2) \, , \tag{39}$$

Here, in order to perform the ensemble average, we have also averaged the integrand over a period $\Delta\tau = 2\pi/k$, assuming ergodicity.
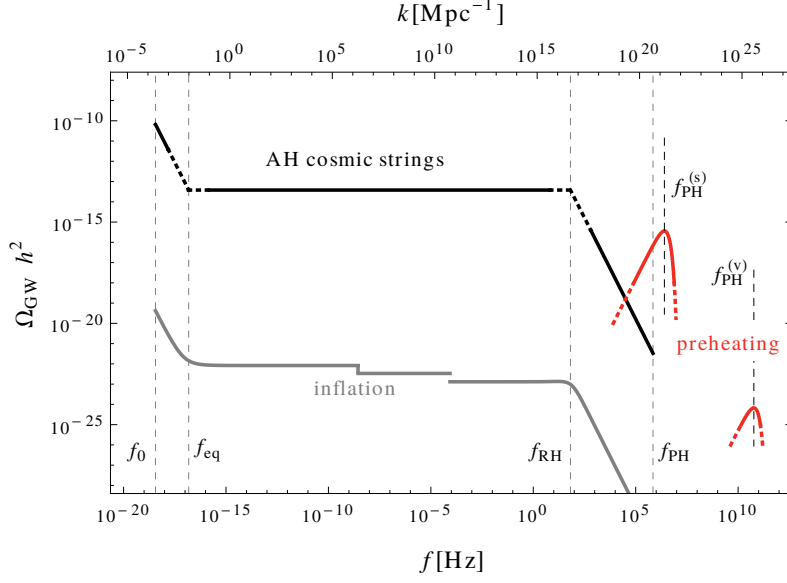
Fig. 10: Predicted GW spectrum due to inflation (grey), preheating (red) and Abelian Higgs cosmic strings (black) for $M_1 = 5.4 \times 10^{10}$ GeV, $v_{B-L} = 5 \times 10^{15}$ GeV and $m_S = 3 \times 10^{13}$ GeV, as in Fig. 5. f_0, $f_{\rm eq}$, $f_{\rm RH}$ and $f_{\rm PH}$ denote the frequencies associated with a horizon-sized wave today, at matter-radiation equality, at reheating and at preheating, respectively. $f_{\rm PH}^{(s)}$ and $f_{\rm PH}^{(v)}$ denote the positions of the peaks in the GW spectrum associated with the scalar and the vector boson present at preheating. The dashed segments indicate the uncertainties due to the breakdown of the analytical approximations. From Ref. [34].

5.2 Gravitational waves from a $B-L$ phase transition

We will now in turn discuss the resulting GW background from inflation, from tachyonic preheating and from cosmic strings in the scaling regime, based on the analysis of Ref. [34]. An overview of the resulting contributions is depicted in Fig. 10.

Gravitational waves from inflation

During inflation quantum fluctuations of the metric are generated and stretched to ever larger physical scales so that they eventually cross the Hubble horizon and become classical. Outside the horizon, the amplitudes of these metric perturbations remain preserved and they only begin to evolve again once they re-enter the Hubble horizon after the end of inflation. Inflation hence gives rise to a stochastic background of gravitational waves [88–90] with a spectrum which is determined by the properties of the primordial quantum metric fluctuations as well as by the expansion history of the universe, which governs the red-shift of the GWs since horizon re-entry,

$$\Omega_{\rm GW}(k,\tau) = \frac{A_t}{12} \frac{k^2}{a_0^2 H_0^2} T_k^2(\tau) \,. \tag{40}$$

Here A_t, controlled by the Hubble parameter during inflation, denotes the amplitude of the primordial tensor perturbations. Evaluating the evolution of the scale factor throughout the cosmic history, i.e. through the epochs of reheating, radiation, matter and vacuum domination, yields the transfer function T_k and thus

$$\Omega_{\rm GW}(k) = \frac{A_t^2}{12} \, \Omega_r \, \frac{g_*^k}{g_*^0} \left(\frac{g_{*,s}^0}{g_{*,s}^k}\right)^{4/3} \times \begin{cases} \frac{1}{2} \left(k_{\rm eq}/k\right)^2 \,, & k_0 \ll k \ll k_{\rm eq} \\ 1 \,, & k_{\rm eq} \ll k \ll k_{\rm RH} \\ 2 \, R \, C_{\rm RH}^6 \, (k_{\rm RH}/k)^2 \,, & k_{\rm RH} \ll k \ll k_{\rm PH} \end{cases} \,, \tag{41}$$

66

with Ω_r denoting the fraction of energy stored in radiation today. The parameters $C_{\rm RH}$ and R account for the deviation from pure matter domination during reheating and the production of relativistic degrees of freedom after $a_{\rm RH}$, respectively, and are numerically found to be typically $\mathcal{O}(1)$.[11] As long as a mode with wave number k re-enters the Hubble horizon during radiation domination, g_*^k and $g_{*,s}^k$ denote the usual values of the effective number of degrees of freedom $g_*(\tau)$ and $g_{*,s}(\tau)$ at time τ_k. On the other hand, during reheating and matter domination g_*^k and $g_{*,s}^k$ correspond to $g_*^{\rm RH}$ and $g_{*,s}^{\rm RH}$ as well as to $g_*^{\rm eq}$ and $g_{*,s}^{\rm eq}$, respectively. The wave numbers $k_{\rm eq}$, $k_{\rm RH}$ and $k_{\rm PH}$ refer to the modes which crossed the horizon at matter-radiation equality, the end of reheating and at preheating, respectively. k_0 is correspondingly given by the size of the Hubble horizon today. Translated into frequencies $f = k/(2\pi a_0)$ at which GW experiments could observe the corresponding modes, they are given by

$$f_0 = 3.58 \times 10^{-19}\,{\rm Hz}\left(\frac{h}{0.70}\right), \qquad f_{\rm eq} = 1.57 \times 10^{-17}\,{\rm Hz}\left(\frac{\Omega_m h^2}{0.14}\right), \tag{42}$$

$$f_{\rm RH} = 4.25 \times 10^{-1}\,{\rm Hz}\left(\frac{T_*}{10^7\,{\rm GeV}}\right), \quad f_{\rm PH} = 1.93 \times 10^4\,{\rm Hz}\left(\frac{\lambda}{10^{-4}}\right)^{1/6}\left(\frac{10^{-15}\,v_{B-L}}{5\,{\rm GeV}}\right)^{2/3}\left(\frac{T_*}{10^7\,{\rm GeV}}\right)^{1/3}, \tag{43}$$

with Ω_m denoting the present value of the fraction of energy stored in matter and T_* closely related to the reheating temperature, see footnote 12. Evidently, the energy spectrum $\Omega_{\rm GW}$ decreases like k^{-2} at its edges and features a plateau in its center, cf. grey curve in Fig. 10. In the context of cosmological $B-L$ breaking, the height of the plateau is controlled by the coupling λ, which determines the self-interaction of the $B-L$ breaking Higgs field, as well as by the $B-L$ breaking scale,

$$\Omega_{\rm GW}^{\rm pl}h^2 = 3.28 \times 10^{-22}\left(\frac{\lambda}{10^{-4}}\right)\left(\frac{v_{B-L}}{5 \times 10^{15}\,{\rm GeV}}\right)^4\left(\frac{\Omega_r}{8.5 \times 10^{-5}}\right)\bar{g}^k, \tag{44}$$

where $\bar{g}^k = (4g_*^k/427)(427/(4g_{*,s}^k))^{4/3}$ is a ratio of energy and entropy degrees of freedom. The small steps visible in the plateau of the grey curve in Fig. 10 represent the change of the number of relativistic degrees of freedom due to the QCD phase transition and the crossing of a typical mass-scale for super-symmetric particles. A remarkable feature of the GW spectrum from inflation is that the position of the kink, which separates the plateau arising for modes which entered during radiation domination and the k^{-2} behaviour from the reheating regime, is directly related to the reheating temperature, providing a possibility to probe this otherwise experimentally hardly accessible quantity.[12]

Gravitational waves from preheating

The process of tachyonic preheating forms a classical, sub-horizon source for GWs which is active only for a short time. The resulting GW spectrum can be obtained by calculating the solution to the mode equation, Eq. (37), and inserting it into Eq. (33). The anisotropic stress tensor Π_{ij} entering Eq. (37) is determined by the dynamics of preheating and vanishes after the end of preheating, allowing the GWs to propagate freely for $\tau \gg \tau_{\rm PH}$. The remaining challenge is thus to calculate Π_{ij} during preheating. This task can be performed numerically, see e.g. Ref. [91] for a detailed description of the method and an application to preheating after chaotic inflation, as well as Ref. [92] for an application to tachyonic preheating after hybrid inflation. Based on analytical estimates supported by the results of these simulations [53, 91–94], one finds two high-frequency peaks in the resulting GW spectrum, related to the

---

[11]For a more detailed discussion of the numerical results, including the precise shape of the 'kinks' in the inflationary GW spectrum, cf. Ref. [34].

[12]To be more precise, the quantity which is probed is the temperature $\hat{T}_{\rm RH}$ when the energy stored in relativistic degrees of freedom (MSSM particles and nonthermal (s)neutrinos) overcomes the energy stored in the non-relativistic $B-L$ Higgs bosons. The quantity T_* appearing in Eq. (43) is related to $\hat{T}_{\rm RH}$ via two correction factors D and R, $T_* = R^{1/2}D^{1/3}\hat{T}_{\rm RH}$. Here D accounts for the entropy production after $a = a_{\rm RH}$ and, just as R, is typically found to be $\mathcal{O}(1)$ by numerically solving the Boltzmann equations.

mass of the $B-L$ vector (v) and scalar Higgs (s) bosons at preheating. The corresponding positions and amplitudes of the peaks in the GW spectrum are given by

$$f_{\mathrm{PH}}^{(s)} \simeq 6.3 \times 10^6 \text{ Hz} \left(\frac{M_1}{10^{11} \text{ GeV}} \right)^{1/3} \left(\frac{5 \times 10^{15} \text{ GeV}}{v_{B-L}} \right)^2 \left(\frac{m_S}{3 \times 10^{13} \text{ GeV}} \right)^{7/6} ,$$

$$\Omega_{\mathrm{GW}}^{(s,\mathrm{max})} h^2 \simeq 3.6 \times 10^{-16} \frac{c_{\mathrm{PH}}}{0.05} \left(\frac{M_1}{10^{11} \text{ GeV}} \right)^{4/3} \left(\frac{5 \times 10^{15} \text{ GeV}}{v_{B-L}} \right)^{-2} \left(\frac{m_S}{3 \times 10^{13} \text{ GeV}} \right)^{-4/3} ,$$

$$f_{\mathrm{PH}}^{(v)} \simeq 7.5 \times 10^{10} \text{ Hz } g \left(\frac{M_1}{10^{11} \text{ GeV}} \right)^{1/3} \left(\frac{m_S}{3 \times 10^{13} \text{ GeV}} \right)^{-1/2} ,$$

$$\Omega_{\mathrm{GW}}^{(v,\mathrm{max})} h^2 \simeq 2.6 \times 10^{-24} \frac{1}{g^2} \frac{c_{\mathrm{PH}}}{0.05} \left(\frac{M_1}{10^{11} \text{ GeV}} \right)^{4/3} \left(\frac{5 \times 10^{15} \text{ GeV}}{v_{B-L}} \right)^2 \left(\frac{m_S}{3 \times 10^{13} \text{ GeV}} \right)^2 ,$$

(45)

and are depicted by the red curves in Fig. 10. Here g is the $B-L$ gauge coupling and c_{PH} is a model-dependent numerical factor, found to be $c_{\mathrm{PH}} = 0.05$ in Ref. [53].

Gravitational waves from cosmic strings

We now turn to the third source, namely, cosmic strings in the scaling regime, cf. Sec. 3.2. We here review the calculation of the resulting GW background in the Abelian Higgs (AH) model following Ref. [95]. In Ref. [34], we additionally discuss an alternative approach based on the Nambu-Goto model of cosmic strings. Here, we will merely give the final result of the latter calculation in order to quantify the theoretical uncertainties involved.

The GW background generated by an AH string network can be estimated analytically starting from Eq. (39). Exploiting general properties of the unequal time correlator of a scaling, sub-horizon source as discussed in Ref. [96] and introducing the dimensionless variable $x = k\tau$, we can evaluate the unequal time correlator of the AH string network, $\Pi^2(k, \tau, \tau')$, as

$$\Pi^2(k, \tau, \tau') = \frac{4 v_{B-L}^4}{\sqrt{\tau \tau'}} C^T(x, x') . \tag{46}$$

Here $C^T(x, x')$ is essentially local in time [96], $C^T(x, x') \sim \delta(x - x') \widetilde{C}(x)$, with $\widetilde{C}$ some function which falls off rapidly for $x \gg 1$, i.e. for modes well inside the horizon. Inserting this into Eq. (39) yields

$$\Omega_{\mathrm{GW}}(k) = \frac{k^2}{3\pi^2 H_0^2 a_0^2} \left(\frac{v_{B-L}}{M_{\mathrm{Pl}}} \right)^4 \int_{x_i}^{x_0} dx \, \frac{a^2(x/k)}{a_0^2 x} \widetilde{C}(x) . \tag{47}$$

As a result of the rapid decrease of $\widetilde{C}(x)$ for $x \gg 1$, this integral is dominated by its lower boundary. For scales which entered the Hubble horizon after the $B-L$ phase transition, $x_i = k \tau_k$ is an $\mathcal{O}(1)$ constant. Hence, the k-dependence of Eq. (47) can be traced back to $a(x/k)$. For radiation domination, we have $a(\tau) \simeq \sqrt{\Omega_r} H_0 \tau a_0^2$, where we have neglected the change in the effective number of degrees of freedom. This yields

$$\int_{x_i}^{x_0} dx \, \frac{a^2(x/k)}{a_0^2 x} \widetilde{C}(x) \simeq \frac{\Omega_r H_0^2 a_0^2}{2 k^2} F^r , \tag{48}$$

where F^r is a constant, and therefore a flat spectrum, $\Omega_{\mathrm{GW}} \propto k^0$. For matter domination, one has $a(x/k) \propto k^{-2}$, which yields $\Omega_{\mathrm{GW}} \propto k^{-2}$.

In summary, we can express today's spectrum of GWs from a scaling network of AH cosmic

strings as[13]

$$\Omega_{\mathrm{GW}}(k) \simeq \Omega_{\mathrm{GW}}^{\mathrm{pl}} \times \left\{ \begin{array}{ll} (k_{\mathrm{eq}}/k)^2, & k_0 \ll k \ll k_{\mathrm{eq}} \\ 1, & k_{\mathrm{eq}} \ll k \ll k_{\mathrm{RH}} \\ (k_{\mathrm{RH}}/k)^2, & k_{\mathrm{RH}} \ll k \ll k_{\mathrm{PH}} \end{array} \right. . \tag{49}$$

Here, k_{eq}, k_{RH} and k_{PH} are determined by Eqs. (42), and (43), and the height of the plateau $\Omega_{\mathrm{GW}}^{\mathrm{pl}}$ can be estimated using the result of the numerical simulations in Ref. [95],

$$\Omega_{\mathrm{GW}}^{\mathrm{pl}} h^2 = 4.0 \times 10^{-14} \frac{F^r}{F_{\mathrm{FHU}}^r} \left(\frac{v_{B-L}}{5 \times 10^{15} \mathrm{GeV}} \right)^4 \left(\frac{\Omega_r h^2}{4.2 \times 10^{-5}} \right), \tag{50}$$

where $F_{\mathrm{FHU}}^r = 4.0 \times 10^3$ is the numerical constant determined in Ref. [95] for global cosmic strings. The corresponding constant for local strings is expected to have the same order of magnitude [97].

Eq. (49) strikingly resembles the result found for the stochastic GW background from inflation, cf. Eq. (41), up to an overall normalization factor, cf. Fig. 10. Note, however, that the origin is quite different. On the one hand, in the case of inflation, the GWs can be traced back to vacuum fluctuations of the metric which remain 'frozen' outside the horizon. After horizon re-entry, they propagate according to the source-free wave equation in FRW space. The amplitude of the resulting stochastic GW background today is determined by the redshift of these modes after entering the horizon. On the other hand, the GWs from cosmic strings stem from a classical source, which is active until today. Only the nature of the unequal time correlator, with its rapid decrease for $x \gg 1$, effectively removes the impact of the source when the corresponding mode is well within the horizon. In more physical terms, this implies that the dominant source for GWs from cosmic strings are Hubble-sized structures of the cosmic string network. This explains why the wave numbers associated with the horizon at a_{RH} and a_{eq} play crucial roles in the GW spectrum from AH cosmic strings, although the GW modes associated with cosmic strings never actually 'cross' the horizon. For cosmic strings the height of the plateau is enhanced by a very large numerical factor F^r. On the contrary, GWs from inflation are suppressed by the small Yukawa coupling λ. This explains the enormous difference in amplitude between GWs from inflation and cosmic strings.

The calculation presented here, resulting in Eq. (49), was based on the Abelian Higgs (AH) cosmic string model. For comparison, Fig. 11 shows the result obtained in the Nambu-Goto (NG) model, cf. Ref. [34]. In both approaches the radiation-dominated epoch leads to a plateau for intermediate frequencies. Compared to the AH result, the boundaries in the NG case are shifted to higher frequencies by a factor $1/\alpha$, where α denotes the size at which cosmic string loops are formed relative to the respective horizon size.[14] This shift in frequency is directly related to the maximal loop size which is determined by αH^{-1} in the NG case. Furthermore, the frequency dependence for small and large frequencies differs, which is a consequence of the different mechanisms of gravitational radiation: in the AH model the dominant contribution to the GW background comes from Hubble-sized structures, in the NG model the dominant contribution is due to 'cusps' in small cosmic string loops, which are formed when waves moving in opposite directions on the loop collide. The striking difference in amplitude by five orders of magnitude between the AH and NG model is due to the different energy loss mechanisms of the string network in the scaling regime. While the energy loss of AH strings is mainly due to massive radiation, NG strings deposit all their energy into GWs. Hence, these two cases provide lower and upper bounds on the GW background from cosmic strings, and it is conceivable that the true answer corresponds to some intermediate value. Assuming a transition between the AH model at early times and the NG model

---

[13]Note that in Eq. (49), the normalization of the '$1/k^2$-flanks' was obtained by matching to the plateau value for $k = k_{\mathrm{RH}}$ and $k = k_{\mathrm{eq}}$, respectively. However, since close to these points the dominant component of the energy density is not much larger than the other components, a more detailed knowledge of $\widetilde{C}(x)$ is necessary to evaluate Eq. (47) at these points.

[14]Note that α cannot take arbitrarily small values. A lower bound is given by the requirement that, in the area of application of the NG model, the loop size should be larger than the string width obtained in the AH model (controlled by m_S^{-1}, m_G^{-1}) or at the very least larger than M_P^{-1}.
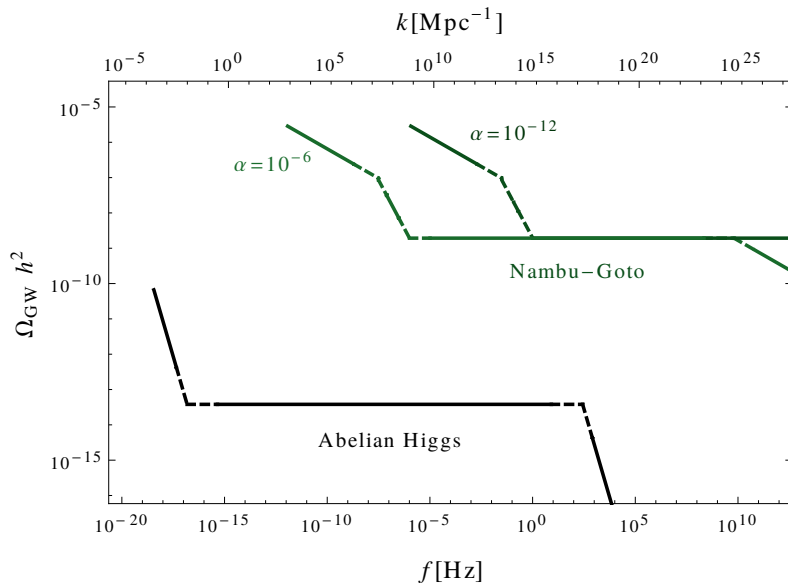
Fig. 11: Comparison of the GW spectra predicted by AH strings and NG strings for two values of α (which governs the initial cosmic string loop size in the NG model). The other parameters are chosen as in Fig. 10, which yields a cosmic string tension of $G\mu = 2 \times 10^{-7}$. From Ref. [34].

at later times sometime during radiation domination, a notable point is that, due to the shift of the GW spectrum of NG strings to higher frequencies, the GWs generated at later times in the NG regime might cover up the GWs generated at earlier times in the AH regime. To address this important question of how to correctly describe the evolution of cosmic strings is clearly a theoretical challenge.

6 Observational Prospects and Outlook

In this paper we have demonstrated that the MSM, a minimal supersymmetric extension of the Standard Model with right-handed neutrinos and spontaneously broken local $B-L$ symmetry, is capable of remedying several shortcomings of the Standard Model while at the same time successfully accounting for the earliest phases of the cosmological evolution. While the MSM allows for grand unification and explains the smallness of the observed neutrino masses on the particle physics side, it accommodates inflation and the generation of entropy, baryon asymmetry and dark matter during the reheating process on the cosmology side. These successes of the MSM therefore truly render it a minimal consistent model of particle physics *and* the early universe.

The MSM gives rise to a rich phenomenology that can be probed in on-going and upcoming cosmological observations and high energy physics experiments. First of all, future data on the temperature anisotropies as well as on the polarization of the CMB radiation will test the dynamics of the $B-L$ breaking sector of the MSM. Dedicated experiments searching for tensor modes in the CMB, such as CMBPol [98] or LiteBIRD [99], have, for instance, the potential to rule out supersymmetric F-term hybrid inflation by measuring a tensor-to-scalar ratio r of $\mathcal{O}(10^{-2})$ or larger, cf. Eq. (10). Meanwhile, indications in the CMB for the presence of local cosmic strings could provide evidence in favour of cosmological $B-L$ breaking, cf. Sec. 3.2. For parameter values compatible with inflation, the AH model of the $B-L$ phase transition typically predicts a cosmic string tension $G\mu$ only shortly below the current observational bound, $G\mu < 3.2 \times 10^{-7}$. From the perspective of the MSM, it is thus expected that signs of cosmic strings should soon be seen.

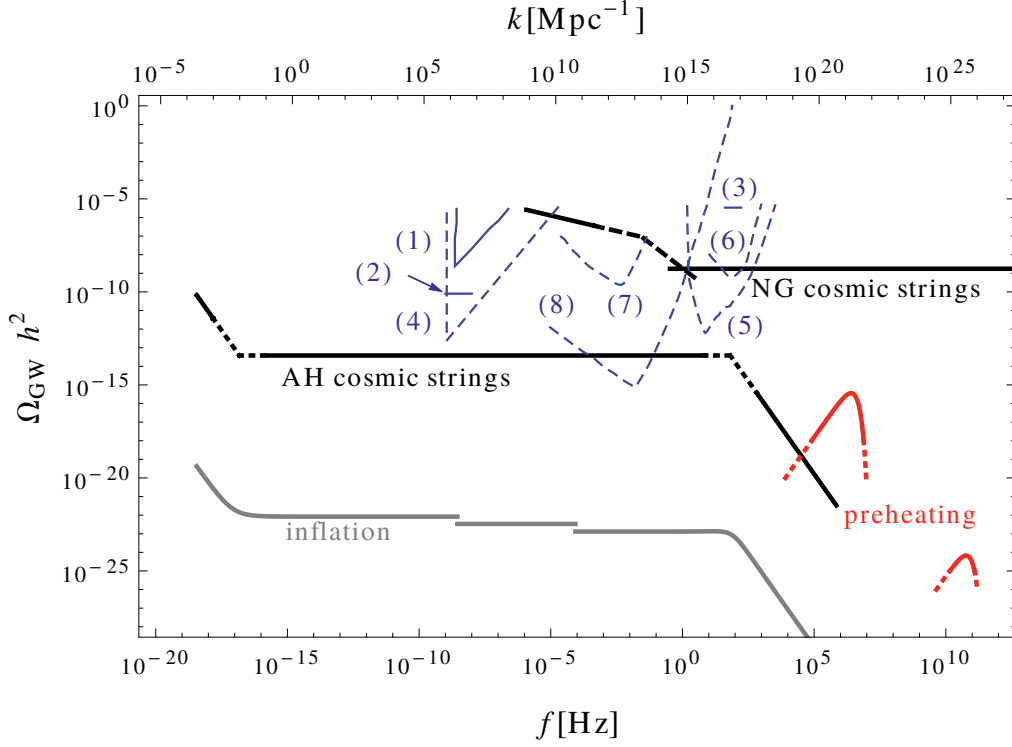Next to the CMB, cosmic strings ought to reveil their existence also in weak and strong lensing

Fig. 12: Predicted GW spectrum and the (expected) sensitivity of current and upcoming experiments. The GW spectrum due to inflation (gray), preheating (red) as well as AH and NG cosmic strings (black) is shown for $v_{B-L} = 5 \times 10^{15}\,\text{GeV}$, $M_1 = 10^{11}\,\text{GeV}$, $m_S = 3 \times 10^{13}\,\text{GeV}$, and $\alpha = 10^{-12}$. The current bounds on the stochastic GW spectrum from (1) millisecond pulsar timing (taken from Ref. [88], with (2) marking the update from EPTA [100] and (3) LIGO [101] are marked by solid blue lines. The dashed blue lines mark the expected sensitivity of some planned experiments: (4) SKA [102], (5) ET [103], (6) advanced LIGO [103], (7) eLISA [104], (8) BBO and DECIGO [105]. Note that with a correlation analysis ultimate DECIGO has a sensitivity down to 10^{-18}. From Ref. [34]

surveys, in the spectrum of ultra-high-energy cosmic rays and GeV-scale γ-rays and finally also in the spectrum of GWs. In Sec. 5, we discussed this latter characteristic signature of the MSM in more detail. In doing to, we put a particular emphasis on the uncertainties in the theoretical calculations, which we assessed by calculating the spectrum of GWs either emitted by AH or by NG cosmic strings. Our result for the GW spectrum related to cosmological $B-L$ breaking is shown in Fig. 12, which compares the GW signals that are respectively expected to originate from AH strings, NG strings, inflation and preheating. In addition to that, Fig. 12 also indicates current bounds on $\Omega_{\text{GW}}h^2$ as well as the expected sensitivity of upcoming GW experiments, cf. Ref. [106] for a review. The observation of a GW signal coming from cosmic strings in the scaling regime in the not too far future is clearly challenging. Depending on the parameters of the AH model, the reheating temperature and the cosmic string loop parameter α, future experiments will either see a flat plateau in the GW spectrum or detect a kink-type feature related to the transition between two successive stages in the expansion history of the universe. Particularly intriguing in this context is the possibility to determine the reheating temperature by measuring the position of the kink in the GW spectrum that is incuded by AH strings at frequencies around f_{RH}, cf. Eq. (43) and footnote 12. Nonetheless it is important to realize that at present our understanding of the formation, evolution and decay of cosmic strings is still far from complete. For one reason or another, the GW background due to cosmic strings might be suppressed or even absent, cf. Ref. [34] for details, thereby

potentially rendering inflation and preheating the dominant sources of GWs. At least in the case of inflation, the exact shape of the GW spectrum and in particular of its kinks could then be predicted with a much better precision than as for cosmic strings [34]. As both the GW signals from inflation as well as from preheating are however rather faint, a positive observation by any of the planned GW experiments seems to be out of reach.

The dynamics of the neutrino sector in the MSM can be tested on the basis of the parameter relations that we derived in our study of the reheating process, cf. Sec. 4.2. Assuming the gravitino to be the LSP, the requirement of consistency between leptogenesis and gravitino dark matter provided us with relations between the neutrino mass parameters $\widetilde{m}_1$ and M_1 on the one hand and the superparticle masses $m_{\widetilde{G}}$ and $m_{\tilde{g}}$ on the other hand, cf. Fig. 8. In particular, we found a lower bound on the gravitino mass that scales quadratically with the gluino mass and that at the same time slightly varies with $\widetilde{m}_1$, cf. Eq. (26). As an alternative to gravitino dark matter, we also considered the possibility of very heavy gravitinos, in the case of which dark matter is accounted for by partly thermally, partly nonthermally produced winos or higgsinos. In this scenario, requiring consistency between leptogenesis, WIMP dark matter and primordial nucleosynthesis, we were able to derive upper bounds on the neutralino mass m_{LSP} as well as absolute lower bounds on the gravitino mass as functions of $\widetilde{m}_1$, cf. Fig. 9.

Owing to these relations and bounds, a determination of $\widetilde{m}_1$, M_1, $m_{\widetilde{G}}$, $m_{\tilde{g}}$ and/or m_{LSP} in present or upcoming experiments would therefore allow to constrain the parameter space of the MSM or even to falsify it. The absolute mass scale of the Standard Model neutrinos, which is closely related to $\widetilde{m}_1$, is, for instance, probed by low-energy neutrino experiments such as GERDA [107] and KATRIN [108] that are looking for neutrinoless double-β decay and studying the β-decay of tritium, respectively. Meanwhile, it is hard to experimentally access the neutrino mass M_1 directly; but fortunately the MSM offers a possibility to determine M_1 indirectly. As reheating after inflation is driven by the decay of heavy (s)neutrinos in the MSM, the plateau temperature T_{RH}^N turns out to be a function of $\widetilde{m}_1$ and M_1, cf. Ref. [10] for details. Once $\widetilde{m}_1$ is known, there thus exists a one-to-one relation between values of M_1 and T_{RH}^N, at least as long as all Yukawa couplings are kept fixed. As mentioned above, it is conceivable that the reheating temperature could possibly be determined by means of GW observations. Such an observation would then also allow for a measurement of M_1.

Depending on the scale of soft supersymmetry breaking and the details of the superparticle mass spectrum, a determination of $m_{\widetilde{G}}$, $m_{\tilde{g}}$ and m_{LSP} is potentially within the reach of experiments aiming at the direct or indirect detection of dark matter and/or collider searches for supersymmetry. If dark matter should be composed of gravitino LSPs, direct and indirect detection experiments would actually be bound to yield null observations. However, if R parity was slightly violated, gravitino dark matter would be unstable [109,110], which could lead to observable signals in the fluxes of gamma rays, charged cosmic rays and cosmic neutrinos [111]. At the same time, the decays of the next-to-lightest superparticle (NLSP) via its R parity-violating interactions might be observable in collider experiments in the form of displaced vertices with distinctive decay signatures [112, 113]. A slight violation of R parity is in fact motivated from cosmology—if R parity was exactly conserved, the late-time decays of the NLSP could spoil the successful predictions of primordial nucleosynthesis [?, 47]—and hence we are confident that the nature of dark matter is not doomed to remain obscure, even if it is made out of gravitinos. Finally, dark matter composed of partly thermally, partly nonthermally produced winos or higgsinos could soon be seen in indirect detection experiments such as H.E.S.S. and Fermi-LAT, cf. footnote 9. On the other hand, for the hierarchical superparticle mass spectrum in Eq. (27), the prospects for a direct detection of WIMP dark matter via its scattering off heavy nuclei do not look particularly promising, cf. Ref. [32]. Also the discovery of a wino or higgsino LSP at colliders seems to be rather challenging in this scenario. Given the large masses for the gluinos and squarks, the characteristic missing energy signature of events with LSPs in the final state may be absent. On the contrary, the wino- or higgsino-like chargino, almost mass degenerate with its neutral partner, might leave macroscopic charged tracks in the detector, which could increase the discovery potential of this dark matter scenario. In addition to that, monojets caused

by the Drell-Yan production of LSP pairs in association with intial state gluon radiation may also provide a possible discovery channel. We therefore conclude that the MSM is experimentally accessible not only in cosmological observations, but also in a number of high energy physics experiments. Upcoming data will thus shed more light on whether or not the MSM is indeed a good description of particle physics up to the multi-TeV scale as well as of the earliest phases of our universe.

Before concluding, we would still like to compare the MSM with a closely related model, the νMSM [115], the non-supersymmetric minimal Standard Model with right-handed neutrinos, which can also account for inflation, entropy production, baryon asymmetry and dark matter. The νMSM is a model with minimal particle content as well as minimal symmetry. The local symmetry is that of the Standard Model and the global $B-L$ symmetry is explicitly broken by Majorana masses of the right-handed neutrinos. Baryogenesis via leptogenesis and dark matter require these masses to lie in the keV and GeV range, far below the electroweak scale, which leads to predictions that are experimentally testable in the near future. The Higgs field of electroweak symmetry breaking also plays the role of the inflaton, which requires a large non-minimal coupling to gravity, tuned to account for the observed amplitude of the CMB temperature anisotropies. In the νMSM there is no unification of strong and electroweak interactions. Also the MSM has minimal matter content. However, the symmetry group is enlarged, and in addition to the Standard Model gauge group it contains local $U(1)_{B-L}$ symmetry and local supersymmetry. Assuming quark and lepton mass matrices compatible with grand unification, and therefore hierarchical right-handed neutrinos, one finds that $U(1)_{B-L}$ is broken at the GUT scale. The symmetry breaking sector contains an inflaton field and the GUT scale automatically yields the right order of magnitude for the amplitude of CMB temperature anisotropies. The lightest superparticle is the constituent of dark matter, which can be searched for at the Large Hadron Collider as well as with direct and indirect detection experiments. Direct evidence for the MSM may eventually be obtained via the spectrum of relic GWs. In summary, supporting evidence for or falsification of the νMSM or the MSM will decide whether or not physics beyond the Standard Model is tied to symmetries larger than those already revealed by the Standard Model.

References

[1] J. Beringer *et al.* [Particle Data Group Collaboration], Phys. Rev. D **86** (2012) 010001.

[2] G. Aad *et al.* [ATLAS Collaboration], Phys. Lett. B **716** (2012) 1 [arXiv:1207.7214 [hep-ex]].

[3] S. Chatrchyan *et al.* [CMS Collaboration], Phys. Lett. B **716** (2012) 30 [arXiv:1207.7235 [hep-ex]].

[4] H. Pagels and J. R. Primack, Phys. Rev. Lett. **48**, 223 (1982).

[5] H. Goldberg, Phys. Rev. Lett. **50**, 1419 (1983) [Erratum-ibid. **103**, 099905 (2009)].

[6] J. R. Ellis, J. S. Hagelin, D. V. Nanopoulos, K. A. Olive and M. Srednicki, Nucl. Phys. B **238**, 453 (1984).

[7] M. Fukugita and T. Yanagida, Phys. Lett. B **174**, 45 (1986).

[8] E. J. Copeland, A. R. Liddle, D. H. Lyth, E. D. Stewart and D. Wands, Phys. Rev. D **49**, 6410 (1994), [astro-ph/9401011].

[9] G. R. Dvali, Q. Shafi and R. K. Schaefer, Phys. Rev. Lett. **73**, 1886 (1994), [hep-ph/9406319].

[10] W. Buchmuller, V. Domcke and K. Schmitz, Nucl. Phys. B **862**, 587 (2012) [arXiv:1202.6679 [hep-ph]].

[11] W. Buchmuller, K. Schmitz and G. Vertongen, Phys. Lett. B **693**, 421 (2010) [arXiv:1008.2355 [hep-ph]].

[12] W. Buchmuller, K. Schmitz and G. Vertongen, Nucl. Phys. B **851**, 481 (2011) [arXiv:1104.2750 [hep-ph]].

[13] M. Plumacher, Nucl. Phys. B **530**, 207 (1998), [hep-ph/9704231].

[14] W. Buchmuller, P. Di Bari and M. Plumacher, Annals Phys. **315**, 305 (2005), [hep-ph/0401240].

[15] G. Lazarides and Q. Shafi, Phys. Lett. B **258**, 305 (1991).

[16] T. Asaka, K. Hamaguchi, M. Kawasaki and T. Yanagida, Phys. Lett. B **464**, 12 (1999), [hep-ph/9906366].

[17] T. Asaka, K. Hamaguchi, M. Kawasaki and T. Yanagida, Phys. Rev. D **61**, 083512 (2000), [hep-ph/9907559].

[18] F. Hahn-Woernle and M. Plumacher, Nucl. Phys. B **806**, 68 (2009),arXiv:0801.3972 [hep-ph].

[19] H. Murayama, H. Suzuki, T. Yanagida and J. Yokoyama, Phys. Rev. Lett. **70**, 1912 (1993).

[20] J. R. Ellis, M. Raidal and T. Yanagida, Phys. Lett. B **581**, 9 (2004),[hep-ph/0303242].

[21] S. Antusch, M. Bastero-Gil, S. F. King and Q. Shafi, Phys. Rev. D **71**, 083519 (2005), [hep-ph/0411298].

[22] S. Antusch, J. P. Baumann, V. F. Domcke and P. M. Kostka, JCAP **1010**, 006 (2010), arXiv:1007.0708 [hep-ph].

[23] V. N. Senoguz and Q. Shafi, hep-ph/0512170.

[24] S. Weinberg, Phys. Rev. Lett. **48**, 1303 (1982).

[25] J. R. Ellis, D. V. Nanopoulos and S. Sarkar, Nucl. Phys. B **259**, 175 (1985).

[26] M. Kawasaki, K. Kohri and T. Moroi, Phys. Lett. B **625**, 7 (2005), [astro-ph/0402490].

[27] M. Kawasaki, K. Kohri and T. Moroi, Phys. Rev. D **71**, 083502 (2005), [astro-ph/0408426].

[28] K. Jedamzik, Phys. Rev. D **74**, 103509 (2006), [hep-ph/0604251].

[29] M. Bolz, W. Buchmuller and M. Plumacher, Phys. Lett. B **443**, 209 (1998), [hep-ph/9809381].

[30] T. Gherghetta, G. F. Giudice and J. D. Wells, Nucl. Phys. B **559** (1999) 27 [hep-ph/9904378].

[31] M. Ibe, R. Kitano, H. Murayama and T. Yanagida, Phys. Rev. D **70** (2004) 075012 [hep-ph/0403198].

[32] W. Buchmuller, V. Domcke and K. Schmitz, Phys. Lett. B **713**, 63 (2012) [arXiv:1203.0285 [hep-ph]].

[33] G. N. Felder, J. Garcia-Bellido, P. B. Greene, L. Kofman, A. D. Linde and I. Tkachev, Phys. Rev. Lett. **87**, 011601 (2001) [hep-ph/0012142].

[34] W. Buchmuller, V. Domcke, K. Kamada and K. Schmitz, arXiv:1305.3392 [hep-ph].

[35] P. A. R. Ade *et al.* [Planck Collaboration], arXiv:1303.5082 [astro-ph.CO].

[36] A. D. Linde and A. Riotto, Phys. Rev. D **56**, 1841 (1997) [hep-ph/9703209].

[37] K. Schmitz, arXiv:1307.3887 [hep-ph].

[38] P. A. R. Ade *et al.* [Planck Collaboration], arXiv:1303.5085 [astro-ph.CO].

[39] W. Buchmuller, L. Covi and D. Delepine, Phys. Lett. B **491**, 183 (2000) [hep-ph/0006168].

[40] K. Nakayama, F. Takahashi and T. T. Yanagida, JCAP **1012**, 010 (2010) [arXiv:1007.5152 [hep-ph]].

[41] C. Pallis and Q. Shafi, arXiv:1304.5202 [hep-ph].

[42] M. Bastero-Gil, S. F. King and Q. Shafi, Phys. Lett. B **651**, 345 (2007) [hep-ph/0604198].

[43] M. Kawasaki, F. Takahashi and T. T. Yanagida, Phys. Lett. B **638**, 8 (2006) [hep-ph/0603265].

[44] M. Endo, F. Takahashi and T. T. Yanagida, Phys. Lett. B **658**, 236 (2008) [hep-ph/0701042].

[45] M. Y. .Khlopov and A. D. Linde, Phys. Lett. B **138**, 265 (1984).

[46] J. R. Ellis, J. E. Kim and D. V. Nanopoulos, Phys. Lett. B **145**, 181 (1984).

[47] T. Moroi, H. Murayama and M. Yamaguchi, Phys. Lett. B **303**, 289 (1993).

[48] W. Buchmuller, V. Domcke, K. Kamada and K. Schmitz, in preparation

[49] T. W. B. Kibble, J. Phys. A **9**, 1387 (1976).

[50] E. J. Copeland, S. Pascoli and A. Rajantie, Phys. Rev. D **65**, 103517 (2002) [hep-ph/0202031].

[51] J. Garcia-Bellido, M. Garcia Perez and A. Gonzalez-Arroyo, Phys. Rev. D **67**, 103501 (2003) [hep-ph/0208228].

[52] J. Garcia-Bellido and E. Ruiz Morales, Phys. Lett. B **536**, 193 (2002) [hep-ph/0109230].

[53] J. Garcia-Bellido and D. G. Figueroa, Phys. Rev. Lett. **98**, 061302 (2007) [astro-ph/0701014].

[54] J. Berges, D. Gelfand and J. Pruschke, Phys. Rev. Lett. **107**, 061301 (2011) [arXiv:1012.4632 [hep-ph]].

[55] A. Vilenkin, Cambridge University Press (1994).

[56] M. Hindmarsh, Prog. Theor. Phys. Suppl. **190**, 197 (2011) [arXiv:1106.0391 [astro-ph.CO]].

[57] F. Lenz, Lect. Notes Phys. **659**, 7 (2005) [hep-th/0403286].

[58] C. T. Hill, H. M. Hodges and M. S. Turner, Phys. Rev. Lett. **59**, 2493 (1987).

[59] H. J. de Vega and F. A. Schaposnik, Phys. Rev. D **14**, 1100 (1976).

[60] M. Hindmarsh, S. Stuckey and N. Bevis, Phys. Rev. D **79**, 123504 (2009) [arXiv:0812.1929 [hep-th]].

[61] S. Kuroyanagi, K. Miyamoto, T. Sekiguchi, K. Takahashi and J. Silk, Phys. Rev. D **87**, 023522 (2013) [arXiv:1210.2829 [astro-ph.CO]].

[62] G. Sigl, K. Jedamzik, D. N. Schramm and V. S. Berezinsky, Phys. Rev. D **52**, 6682 (1995) [astro-ph/9503094].

[63] R. J. Protheroe and T. Stanev, Phys. Rev. Lett. **77**, 3708 (1996) [Erratum-ibid. **78**, 3420 (1997)] [astro-ph/9605036].

[64] P. Bhattacharjee, Q. Shafi and F. W. Stecker, Phys. Rev. Lett. **80**, 3698 (1998) [hep-ph/9710533].

[65] G. Sigl, S. Lee, P. Bhattacharjee and S. Yoshida, Phys. Rev. D **59**, 043504 (1999) [hep-ph/9809242].

[66] U. F. Wichoski, J. H. MacGibbon and R. H. Brandenberger, Phys. Rev. D **65**, 063005 (2002) [hep-ph/9805419].

[67] J. N. Moore, E. P. S. Shellard and C. J. A. P. Martins, Phys. Rev. D **65**, 023503 (2002) [hep-ph/0107171].

[68] G. Vincent, N. D. Antunes and M. Hindmarsh, Phys. Rev. Lett. **80**, 2277 (1998) [hep-ph/9708427].

[69] A. Albrecht and N. Turok, Phys. Rev. D **40**, 973 (1989).

[70] V. Vanchurin, K. D. Olum and A. Vilenkin, Phys. Rev. D **74**, 063527 (2006) [gr-qc/0511159].

[71] K. D. Olum and V. Vanchurin, Phys. Rev. D **75**, 063521 (2007) [astro-ph/0610419].

[72] J. J. Blanco-Pillado, K. D. Olum and B. Shlaer, Phys. Rev. D **83**, 083514 (2011) [arXiv:1101.5173 [astro-ph.CO]].

[73] W. Buchmuller, R. D. Peccei and T. Yanagida, Ann. Rev. Nucl. Part. Sci. **55**, 311 (2005) [hep-ph/0502169].

[74] E. Komatsu *et al.* [WMAP Collaboration], Astrophys. J. Suppl. **192**, 18 (2011) [arXiv:1001.4538 [astro-ph.CO]].

[75] W. Buchmuller, V. Domcke and K. Schmitz, JHEP **1203**, 008 (2012) [arXiv:1111.3872 [hep-ph]].

[76] P. A. R. Ade *et al.* [Planck Collaboration], arXiv:1303.5076 [astro-ph.CO].

[77] M. Ibe and T. T. Yanagida, Phys. Lett. B **709**, 374 (2012) [arXiv:1112.2462 [hep-ph]].

[78] K. S. Jeong, M. Shimosuka and M. Yamaguchi, JHEP **1209**, 050 (2012) [arXiv:1112.5293 [hep-ph]].

[79] S. Krippendorf, H. P. Nilles, M. Ratz and M. W. Winkler, Phys. Lett. B **712**, 87 (2012) [arXiv:1201.4857 [hep-ph]].

[80] S. P. Martin, In *Kane, G.L. (ed.): Perspectives on supersymmetry II* 1-153 [hep-ph/9709356].

[81] T. Cohen, M. Lisanti, A. Pierce and T. R. Slatyer, arXiv:1307.4082 [hep-ph].

[82] J. Fan and M. Reece, arXiv:1307.4400 [hep-ph].

[83] N. Arkani-Hamed, A. Delgado and G. F. Giudice, Nucl. Phys. B **741**, 108 (2006) [hep-ph/0601041].

[84] J. Hisano, S. Matsumoto, M. Nagai, O. Saito and M. Senami, Phys. Lett. B **646**, 34 (2007) [hep-ph/0610249].

[85] M. Cirelli, A. Strumia and M. Tamburini, Nucl. Phys. B **787**, 152 (2007) [arXiv:0706.4071 [hep-ph]].

[86] B. Allen, In *Les Houches 1995, Relativistic gravitation and gravitational radiation* 373-417 [gr-qc/9604033].

[87] M. Maggiore, Oxford University Press, October 2007. 572p. (ISBN-13: 978-0-19-857074-5)

[88] T. L. Smith, M. Kamionkowski and A. Cooray, Phys. Rev. D **73**, 023504 (2006) [astro-ph/0506422].

[89] M. S. Turner, M. J. White and J. E. Lidsey, Phys. Rev. D **48**, 4613 (1993) [astro-ph/9306029].

[90] K. Nakayama, S. Saito, Y. Suwa and J. 'i. Yokoyama, JCAP **0806**, 020 (2008) [arXiv:0804.1827 [astro-ph]].

[91] J. F. Dufaux, A. Bergman, G. N. Felder, L. Kofman and J. -P. Uzan, Phys. Rev. D **76**, 123517 (2007) [arXiv:0707.0875 [astro-ph]].

[92] J. -F. Dufaux, G. Felder, L. Kofman and O. Navros, JCAP **0903**, 001 (2009) [arXiv:0812.2917 [astro-ph]].

[93] G. N. Felder and L. Kofman, Phys. Rev. D **75**, 043518 (2007) [hep-ph/0606256].

[94] J. -F. Dufaux, D. G. Figueroa and J. Garcia-Bellido, Phys. Rev. D **82**, 083518 (2010) [arXiv:1006.0217 [astro-ph.CO]].

[95] D. G. Figueroa, M. Hindmarsh and J. Urrestilla, Phys. Rev. Lett. **110**, 101302 (2013) [arXiv:1212.5458 [astro-ph.CO]].

[96] R. Durrer, M. Kunz and A. Melchiorri, Phys. Rev. D **59**, 123005 (1999) [astro-ph/9811174].

[97] M. Hindmarsh, private communication.

[98] D. Baumann *et al.* [CMBPol Study Team Collaboration], AIP Conf. Proc. **1141**, 10 (2009) [arXiv:0811.3919 [astro-ph]].

[99] LiteBIRD project, `http://cmb.kek.jp/litebird/index.html`; M. Hazumi, AIP Conf. Proc. **1040**, 78 (2008).

[100] R. van Haasteren, Y. Levin, G. H. Janssen, K. Lazaridis, M. K. B. W. Stappers, G. Desvignes, M. B. Purver and A. G. Lyne *et al.*, arXiv:1103.0576 [astro-ph.CO].

[101] C. Palomba [LIGO Scientific and Virgo Collaborations], arXiv:1201.3176 [astro-ph.IM].

[102] M. Kramer, astro-ph/0409020.

[103] M. Abarnathy, F. Acernese, P. Ajith et al [ET Science Team], "Einstein gravitational wave Telescope - Conceptual Design Study," ET-0106C-10, European Gravitational Observatory, 2011.

[104] P. Amaro-Seoane, S. Aoudia, S. Babak, P. Binetruy, E. Berti, A. Bohe, C. Caprini and M. Colpi *et al.*, arXiv:1201.3621 [astro-ph.CO].

[105] L. Alabidi, K. Kohri, M. Sasaki and Y. Sendouda, JCAP **1209**, 017 (2012) [arXiv:1203.4663 [astro-ph.CO]].

[106] M. Maggiore, Phys. Rept. **331**, 283 (2000) [gr-qc/9909001].

[107] M. Agostini *et al.* [GERDA Collaboration], arXiv:1307.4720 [nucl-ex].

[108] [for the KATRIN Collaboration], arXiv:1307.5486 [physics.ins-det].

[109] F. Takayama and M. Yamaguchi, Phys. Lett. B **485**, 388 (2000) [hep-ph/0005214].

[110] W. Buchmuller, L. Covi, K. Hamaguchi, A. Ibarra and T. Yanagida, JHEP **0703**, 037 (2007) [hep-

ph/0702184 [HEP-PH]].

[111] M. Grefe, arXiv:1111.6779 [hep-ph].

[112] S. Bobrovskyi, W. Buchmuller, J. Hajer and J. Schmidt, JHEP **1109**, 119 (2011) [arXiv:1107.0926 [hep-ph]].

[113] S. Bobrovskyi, J. Hajer and S. Rydbeck, JHEP **1302**, 133 (2013) [arXiv:1211.5584 [hep-ph]].

[114] A. de Gouvea, T. Moroi and H. Murayama, Phys. Rev. D **56**, 1281 (1997) [hep-ph/9701244].

[115] For a review and references, see M. Shaposhnikov, Phys. Part. Nucl. **41** (2010) 862.